Fall 2016

Developmental, Physiological, and Transcriptomic Analyses of Neurons involved in the Generation of Mammalian Breathing

andrew Kottick

College of William and Mary - Arts & Sciences, andrewkottick@gmail.com

Recommended Citation

Developmental, Physiological, and Transcriptomic Analyses of Neurons Involved
in the Generation of Mammalian Breathing

Andrew Kottick

Sudbury, Ontario, Canada

Master of Science, University of Calgary, 2011
Bachelor of Science, Laurentian University, 2008

A Dissertation presented to the Graduate Faculty
of the College of William and Mary in Candidacy for the Degree of
Doctor of Philosophy
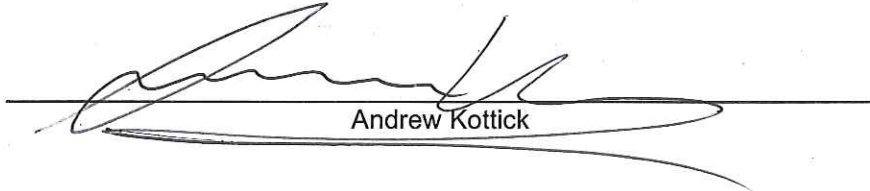
Department of Applied Science

The College of William and Mary
January 2017

APPROVAL PAGE

This Dissertation is submitted in partial fulfillment of
the requirements for the degree of

Doctor of Philosophy

Andrew Kottick

Approved by the Committee, November, 2016
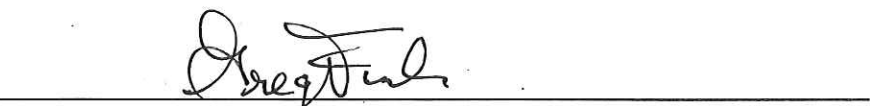
Committee Chair
Professor Christopher A. Del Negro
Department of Applied Science, The College of William & Mary

Chancellor Professor Lizabeth A. Allison
Department of Biology, The College of William & Mary

Chancellor Professor Margaret S. Saha
Department of Biology, The College of William & Mary

Professor Gregory D. Funk
Department of Physiology, University of Alberta

COMPLIANCE PAGE

Research approved by

<u>Institutional Animal Care and Use Committee (IACUC)</u>
<u>The College of William and Mary</u>

Protocol numbers: (1) IACUC-2010-07-12-6795-cadeln

(2) IACUC-2013-07-12-8828-cadeln

(3) IACUC-2013-07-10-8833-cadeln

(4) IACUC 2014-03-12-9412-cadeln

(5) IACUC 2016-08-02-11305-cadeln

(6) IACUC 2016-08-02-11302-cadeln

Dates of approval: (1) 2010-07-30

(2) 2013-07-19

(3) 2013-07-29

(4) 2014-04-16

(5) 2016-08-17

(6) 2016-08-17

ABSTRACT

Breathing is a rhythmic motor behavior with obvious physiological importance: breathing movements are essential for respiration, which sustains homeostasis and life itself in a wide array of animals including humans and all mammals. The breathing rhythm is produced by interneurons of the brainstem preBötzinger complex (preBötC) whose progenitors express the transcription factor Dbx1. However, the cellular and synaptic neural mechanisms underlying respiratory rhythmogenesis remain unclear. The first chapter of this dissertation examines a Dbx1 transgenic mouse line often exploited to study the neural control of breathing. It emphasizes the cellular fate of progenitors that express Dbx1 at different times during development. I couple tamoxifen-inducible Dbx1 Cre-driver mice with Cre-dependent reporters, then show that Dbx1-expressing progenitors give rise to preBötC neurons and glia. Further, I quantify the temporal assemblage of Dbx1 neurons and glia in the preBötC and provide practical guidance on breeding and tamoxifen administration strategies to bias reporter protein expression toward neurons (or glia), which can aid researchers in targeting studies to unravel their functions in respiratory neurobiology. The second chapter of this dissertation exploits the mouse model characterized in the first chapter and then focuses on mechanisms of respiratory rhythmogenesis. The breathing cycle consists of inspiratory and expiratory phases. Inspiratory burst-initiation and burst-sustaining mechanisms have been investigated by many groups. Here, I specifically investigate the role of short-term synaptic depression in burst termination and the inspiratory-expiratory phase transition using rhythmically active medullary slice preparations from Dbx1 Cre-driver mice coupled with channelrhodopsin reporters. I demonstrate the existence of a post-inspiratory refractory period that precludes light-evoked bursts in channelrhodopsin-expressing Dbx1-derived preBötC neurons. I show that postsynaptic factors cannot account for the refractory period, and that presynaptic vesicle depletion most likely underlies the refractory period. The third chapter of this dissertation focuses on transcriptomic analysis of Dbx1 preBötC neurons, and differences in gene expression between Dbx1-derived and non-Dbx1-derived preBötC neurons. I analyze and quantify the expression of over 20,000 genes, and make the raw data publicly available for further analysis. I argue that this full transcriptome approach will enable our research group (and others) to devise physiological studies that target specific subunits of ion channels and integral membrane proteins to examine the role(s) of Dxb1-derived neurons and glia at the molecular level of breathing behavior. In addition to predictable gene candidates (such as ion channels, etc) this transcriptome analysis delivers unanticipated novel gene candidates that can be investigated in future respiratory physiology experiments. Knowing the site (preBötC) and cell class (Dbx1) at the point of origin of respiration, this dissertation provides tools and specific investigations that advance understanding of the neural mechanisms of breathing.

TABLE OF CONTENTS

ACKNOWLEDGEMENTS

I would like to express my sincere gratitude to my Ph.D. advisor, Dr. Christopher Del Negro, who has had a tremendous impact on both my academic and personal life. Christopher has set an example of excellence as a researcher, writer, presenter, and role model. Over the last five years, Christopher has been supportive both as an instructor and as a friend.

I would also like to thank members of the Del Negro lab. I wish to thank fellow Ph.D. student Nikolas Vann, for his technical competence and willingness to help me trouble shoot experiments. I wish to thank Dr. Maria Cristina Picardo, for her help with molecular experiments. I wish to thank Dr. John Hayes for helping me with his encyclopedic knowledge of the respiratory literature and his bioinformatics expertise. And I wish to thank undergraduate students Kaitlyn Dorst and Caroline Martin for helping with animal colony work and immunohistochemistry experiments.

I would like to thank Lydia Whitaker and Lianne Ashburne for helping me navigate the administrative aspects of my Ph.D. studies, and for always having an open door for a good conversation or a laugh. Lydia always went the extra mile to help me, and made my time in the Department of Applied Science truly enjoyable.

Finally, I would like to thank my Ph.D. advisory committee. I wish to thank Dr. Margaret Saha, who has been a supportive colleague, for her work and the work of students in her lab on the RNA-Seq project. I wish to thank Dr. Lizabeth Allison, who I sincerely consider the best course instructor that I've ever had. And I wish to thank Dr. Gregory Funk, a long-time colleague and collaborator, for his input on our manuscripts and feedback on my dissertation.

This Ph.D. dissertation is dedicated to my mother, for her unconditional love and constant support.

LIST OF TABLES

LIST OF FIGURES

Introduction

Rhythmic motor behaviors like walking, chewing, and breathing are controlled by central pattern generator (CPG) networks in the brainstem and spinal cord (Grillner, 2006). CPGs set the tempo and determine appropriate sequences of muscle activation to accomplish each behaviorally specific motor pattern. A major goal for neuroscience is to understand the mechanisms that underlie these behaviors – from gene expression and regulation to cellular and synaptic mechanisms that contribute to rhythm generation and pattern formation.

The CPG for breathing was identified and localized to the ventral medulla twenty-five years ago. More recently, the genetic identity of its constituent rhythmogenic interneurons was discovered. Despite knowing the location and genetic class of neurons that form the core oscillator, the mechanisms that underlie respiratory rhythm generation remain elusive. Thus, we seek innovative tools, like intersectional mouse genetics and transcriptome screening, to probe the cellular and molecular basis of breathing behavior.

The preBötzinger complex (preBötC) is a bilateral network of interneurons in the ventral medulla that contains the core oscillator for inspiratory breathing movements (Smith et al., 1991; Feldman et al., 2013). Rhythmic bursts of activity generated within the preBötC propagate to cranial and spinal motor neurons that innervate inspiratory muscles including the diaphragm, external intercostals, and upper airway muscles (including notably the genioglossus).

The rostral and caudal borders of the preBötC were first functionally defined by transsection experiments in neonatal rats (Smith et al., 1991). Peptides that modulate breathing (as well as their associated receptors) were then identified and used to anatomically localize a population of core rhythmogenic interneurons to the ventral lateral medulla (Gray et al., 1999, 2001; Tan et al., 2008). And recently, the preBötC core was genetically defined as being comprised of interneurons derived from progenitors that express the transcription factor Dbx1.

Dbx1-derived neurons populate the ventral medulla in the region of the preBötC and express peptidergic markers associated with respiratory rhythmogenic function (Bouvier et al., 2010; Gray et al., 2010). Further, Dbx1 knockout mice are born cyanotic – they do not breathe, and no preBötC is formed during development. Dbx1 is currently the best marker for the preBötC core, and is now being exploited as a genetic target for studies addressing the neural control of breathing (Picardo et al., 2013; Wang et al., 2014; Kottick and Del Negro, 2015; Revill et al., 2015; Cui et al., 2016; Koizumi et al., 2016).

In the first chapter of this dissertation, I characterize Dbx1 preBötC expression using a transgenic Cre-driver mouse that is a useful tool to identify and manipulate Dbx1 preBötC neurons for anatomical and physiological experiments. Specifically, I outline the procedure that I used to make the strain homozygous, describe the temporal expression of Dbx1 in progenitors that give

rise to preBötC neurons and glia, compare two Dbx1 Cre-driver lines, and recommend breeding strategies to optimize their use in the context of studying breathing behavior.

Dbx1 preBötC neurons are predominantly glutamatergic, and the only element of rhythmogenesis that is completely agreed upon is that recurrent synaptic excitation via AMPA receptors is critical for respiratory rhythmogenesis (Smith et al., 1990; Funk et al., 1993). Rubin et al. (2009) describe a mathematical model of preBötC rhythm generation (called the *group pacemaker*) in which inspiratory bursts initiated by recurrent excitation are terminated by a combination of activity-dependent outward currents and synaptic depression. Electrophysiology experiments have confirmed the existence of large-magnitude post-inspiratory outward currents in preBötC inspiratory neurons. However, the role of synaptic depression in burst termination has remained an untested hypothesis.

In the second chapter of this dissertation I address the role of synaptic depression in inspiratory-expiratory phase transition and burst termination. Using rhythmically-active medullary slice preparations from neonatal mice, I first identify a post-inspiratory refractory period that precludes light-evoked inspiratory bursts in Dbx1-derived neurons that express channelrhodopsin. I then demonstrate depression of excitatory postsynaptic potentials in Dbx1-derived preBötC neurons by electrically stimulating midline-crossing axons.

Finally, I rule out postsynaptic factors, and show that the depression is likely due to presynaptic vesicle depletion.

The intrinsic membrane properties in preBötC neurons that influence respiratory rhythm generation were characterized using intracellular patch-clamp recordings (Ramirez and Richter, 1996; Feldman et al., 2013; Richter and Smith, 2014). However, testing their relative contributions to rhythmogenesis has relied on promiscuous pharmacology and has often led to inconclusive results. I argue that a comprehensive analysis of gene expression in Dbx1-derived preBötC neurons could be used to develop targeted experiments that influence specific ion channel subunits, pumps, or transporters.

In the third chapter of this dissertation, I provide the first RNA-Seq gene expression profile for preBötC neurons. I determine the presence and quantity of mRNA for over 20,000 protein-encoding genes in both Dbx1-derived, and non-Dbx1-derived preBötC neurons. Further, we performed differential gene expression analysis to elucidate variations in mRNA expression levels between the two populations. These data will be made publicly available in an open-access database, which will enable investigators to exploit these data in custom analyses. This chapter quantifies gene expression in preBötC neurons, and can be used to design hypothesis-driven studies that will address the role of transcription factors and ion channels in preBötC development and rhythm generation.

The studies presented in this dissertation recapitulate the developmental assemblage of Dbx1-derived preBötC cells, illustrate the role of excitatory synaptic mechanisms in respiratory rhythm generation, and provide a roadmap for genetic analysis of the rhythmogenic core of the preBötC. These data can be used to design further experiments to interrogate the cellular composition, structure, and function of the preBötC.

References

Bouvier J, Thoby-Brisson M, Renier N, Dubreuil V, Ericson J, Champagnat J, Pierani A, Chédotal A, Fortin G (2010) Hindbrain interneurons and axon guidance signaling critical for breathing. Nat Neurosci 13:1066–1074.

Cui Y, Kam K, Sherman D, Janczewski WA, Zheng Y, Feldman JL (2016) Defining preBötzinger Complex Rhythm- and Pattern-Generating Neural Microcircuits In Vivo. Neuron 91:602–614.

Feldman JL, Del Negro CA, Gray PA (2013) Understanding the rhythm of breathing: so near, yet so far. Annu Rev Physiol 75:423–452.

Funk GD, Smith JC, Feldman JL (1993) Generation and transmission of respiratory oscillations in medullary slices: role of excitatory amino acids. J Neurophysiol 70:1497–1515.

Gray PA, Hayes JA, Ling GY, Llona I, Tupal S, Picardo MCD, Ross SE, Hirata T, Corbin JG, Eugenín J, Del Negro CA (2010) Developmental origin of preBötzinger complex respiratory neurons. J Neurosci Off J Soc Neurosci 30:14883–14895.

Gray PA, Janczewski WA, Mellen N, McCrimmon DR, Feldman JL (2001) Normal breathing requires preBötzinger complex neurokinin-1 receptor-expressing neurons. Nat Neurosci 4:927–930.

Gray PA, Rekling JC, Bocchiaro CM, Feldman JL (1999) Modulation of Respiratory Frequency by Peptidergic Input to Rhythmogenic Neurons in the PreBötzinger Complex. Science 286:1566–1568.

Grillner S (2006) Biological pattern generation: the cellular and computational logic of networks in motion. Neuron 52:751–766.

Koizumi H, Mosher B, Tariq MF, Zhang R, Koshiya N, Smith JC (2016) Voltage-Dependent Rhythmogenic Property of Respiratory Pre-Bötzinger Complex Glutamatergic, Dbx1-Derived, and Somatostatin-Expressing Neuron Populations Revealed by Graded Optogenetic Inhibition. eNeuro 3.

Kottick A, Del Negro CA (2015) Synaptic Depression Influences Inspiratory-Expiratory Phase Transition in Dbx1 Interneurons of the preBötzinger Complex in Neonatal Mice. J Neurosci Off J Soc Neurosci 35:11606–11611.

Picardo MCD, Weragalaarachchi KTH, Akins VT, Del Negro CA (2013) Physiological and morphological properties of Dbx1-derived respiratory neurons in the pre-Botzinger complex of neonatal mice. J Physiol 591:2687–2703.

Ramirez JM, Richter DW (1996) The neuronal mechanisms of respiratory rhythm generation. Curr Opin Neurobiol 6:817–825.

Revill AL, Vann NC, Akins VT, Kottick A, Gray PA, Del Negro CA, Funk GD (2015) Dbx1 precursor cells are a source of inspiratory XII premotoneurons. eLife 4.

Richter DW, Smith JC (2014) Respiratory rhythm generation in vivo. Physiol Bethesda Md 29:58–71.

Rubin JE, Hayes JA, Mendenhall JL, Del Negro CA (2009) Calcium-activated nonspecific cation current and synaptic depression promote network-dependent burst oscillations. Proc Natl Acad Sci U S A 106:2939–2944.

Smith JC, Ellenberger HH, Ballanyi K, Richter DW, Feldman JL (1991) Pre-Bötzinger complex: a brainstem region that may generate respiratory rhythm in mammals. Science 254:726–729.

Smith JC, Greer JJ, Liu GS, Feldman JL (1990) Neural mechanisms generating respiratory pattern in mammalian brain stem-spinal cord in vitro. I. Spatiotemporal patterns of motor and medullary neuron activity. J Neurophysiol 64:1149–1169.

Tan W, Janczewski WA, Yang P, Shao XM, Callaway EM, Feldman JL (2008) Silencing preBötzinger complex somatostatin-expressing neurons induces persistent apnea in awake rat. Nat Neurosci 11:538–540.

Wang X, Hayes JA, Revill AL, Song H, Kottick A, Vann NC, LaMar MD, Picardo MCD, Akins VT, Funk GD, Del Negro CA (2014) Laser ablation of Dbx1 neurons in the pre-Bötzinger complex stops inspiratory rhythm and impairs output in neonatal mice. eLife 3:e03427.

CHAPTER 1: Fate mapping neurons and glia derived from Dbx1-expressing progenitors in mouse preBötzinger complex

1.1 Abstract

The brainstem preBötzinger complex (preBötC) generates the inspiratory breathing rhythm, and its core rhythmogenic interneurons are derived from Dbx1-expressing progenitors. To study the neural bases of breathing, tamoxifen-inducible Cre-driver mice and Cre-dependent reporters are used to identify, record, and perturb Dbx1 preBötC neurons. However, the relationship between tamoxifen administration and reporter protein expression in preBötC neurons and glia has not been characterized or quantified. To address this problem, we crossed mice that express tamoxifen-inducible Cre recombinase under the control of the $Dbx1$ gene ($Dbx1^{CreERT2}$) with Cre-dependent fluorescent reporter mice ($Rosa26^{tdTomato}$), administered tamoxifen at different times during development, and analyzed tdTomato expression in the preBötC of their offspring. We also crossed $Rosa26^{tdTomato}$ reporters with mice that constitutively express Cre driven by $Dbx1$ ($Dbx1^{Cre}$) and analyzed tdTomato expression in the preBötC of their offspring for comparison. We show that Dbx1-expressing progenitors give rise to preBötC neurons and glia. Peak neuronal tdTomato expression occurs when tamoxifen is administered at embryonic day 9.5 (E9.5), whereas tdTomato expression in glia showed no clear relationship to tamoxifen timing. These results can be used to bias

reporter protein expression in neurons (or to study glia), depending on the experimental objective. From the standpoint of investigating neuronal mechanisms, tamoxifen administration at E9.5 labels 91% of Dbx1-derived neurons in the preBötC yet 46% of Dbx1-derived glia. By fate-mapping Dbx1-expressing progenitors, this study illustrates the developmental assemblage of Dbx1-derived cells in preBötC, which can be used to design intersectional Cre/lox experiments that interrogate its cellular composition, structure, and function.

1.2 Introduction

The brainstem preBötzinger Complex (preBötC) generates the rhythm that drives inspiratory breathing movements in mammals (Smith et al., 1991; Feldman et al., 2013; Moore et al., 2013) and its core rhythmogenic interneurons are derived from progenitors that express the transcription factor Dbx1 (i.e., Dbx1 neurons). The putatively rhythmogenic nature of Dbx1 preBötC neurons was first identified using mice that express *LacZ* under the control of the *Dbx1* gene (Pierani et al., 2001), and the *LacZ* reporter system was used to quantify peptide receptor localization and transmitter phenotypes of Dbx1 preBötC neurons (Bouvier et al., 2010; Gray et al., 2010). Recently, mice that express constitutive Cre (*Dbx1*[Cre]; Bielle et al., 2005) or tamoxifen-inducible Cre (*Dbx1*[CreERT2]; Hirata et al., 2009), both under the control of the *Dbx1* gene, have been used in physiological experiments that address the role of Dbx1 neurons

in respiration (Picardo et al., 2013; Wang et al., 2014; Kottick and Del Negro, 2015; Revill et al., 2015; Cui et al., 2016; Koizumi et al., 2016). Unfortunately, the inducible Cre/lox studies lack cellular data about how the timing of tamoxifen administration affects preBötC reporter protein expression, which introduces ambiguity regarding the absolute quantity or relative proportion of Dbx1-derived preBötC neurons or glia that are being recorded or manipulated.

Here we addressed this problem by breeding $Dbx1^{CreERT2}$ females with male Cre-dependent fluorescent reporter mice ($Rosa26^{tdTomato}$) and administering tamoxifen to pregnant dams at either embryonic day 7.5, 8.5, 9.5, 10.5, or 11.5, which covers the window of Dbx1 expression during embryogenesis. We found that Dbx1-derived progenitors give rise to preBötC neurons and glia, which can be distinguished by molecular markers and morphological criteria. The number of preBötC neurons that expressed tdTomato peaked when tamoxifen was administered at embryonic day 9.5 (E9.5), while the number of preBötC glia that expressed tdTomato was constant across all tamoxifen administration time points.

These data recap the temporal assemblage of Dbx1-derived preBötC cells during embryonic development, and can be applied to bias reporter protein expression in preBötC neurons (or to study glia) to optimize the applicability of $Dbx1^{CreERT2}$ mice for respiratory neurobiology studies.

1.3 Materials and Methods

Animals: All animal procedures were performed in accordance with the [Author University] animal care committee's regulations. Female mice that express a tamoxifen-sensitive Cre recombinase ($Dbx1^{CreERT2}$; CD1 background strain, Hirata et al., 2009) or constitutive Cre recombinase ($Dbx1^{Cre}$; CD1 background strain, Bielle et al., 2005) in cells that express the $Dbx1$ gene were crossed with male mice whose $Rosa26$ locus was modified to express tdTomato fluorescent protein in a Cre-dependent manner ($Rosa26^{tdTomato}$; C57BL/6 background strain, stock no. 007905, Jackson Laboratory; Bar Harbor, ME). Female Cre-driver mice were always crossed with male $Rosa26^{tdTomato}$ mice because CD1 dams yield larger litters (12-16 pups) than C57BL/6 dams (4-10 pups). Tamoxifen (22.5 mg/kg body mass, T5648, Sigma-Aldrich; St. Louis, MO) was administered to pregnant females via oral gavage. Experiments were performed on male and female $Dbx1^{CreERT2}$; $Rosa26^{tdTomato}$ mice aged 6-8 weeks.

Genotyping: RT-PCR for a Cre probe (Transnetyx; Cordova, TN) was performed on tail clippings from the offspring of $Dbx1^{+/CreERT2}$ crosses. The "signal" was calculated by normalizing the raw data from each sample to the housekeeping gene *c-jun* for that sample.

Adeno-associated virus (AAV) injection: $Dbx1^{CreERT2}$; $Rosa26^{tdTomato}$ mice were anesthetized with intraperitoneal injection of ketamine (100 mg/kg body mass) and aseptic surgeries were performed in a stereotaxic apparatus. The

skull was exposed and unilateral craniotomies (0.5 mm diameter) were performed at 7.0 mm posterior to bregma and 1.3 mm lateral to the midline suture. 200 μl of AAV that drives GFP expression via a human synapsin promoter (AAV-hSyn-GFP, AV-9-PV1696, University of Pennsylvania Vector Core; Philadelphia, PA) was injected with a 5-μl syringe (Hamilton; Reno, NV) at a depth of 4.7 mm from the dorsal surface of the brain. Incisions were closed with sutures and mice recovered for 4 days before they were sacrificed.

Tissue clearing: Tissue preparation and passive clearing were performed as described by Treweek et al. (2015). Animals were anesthetized and transcardially perfused with 4% paraformaldehyde. Brainstems were postfixed for 12 h at 4°C and sliced to a thickness of 500 μm. Slices were incubated in A4P1 hydrogel solution in a glass vacutainer tube on a rocking platform for 12 h at 4°C. The tube was evacuated of air for 5 min and the hydrogel solution was bubbled with nitrogen gas for an additional 5 min to purge residual oxygen. Tubes containing the brainstem slices and hydrogel solution were incubated in a 37°C water bath for 3 h. Slices were transferred to SDS clearing buffer and incubated at 37°C on an orbital shaker for 8-12 h, or until sufficiently clear. The tissue was washed in 1x PBS on a rotating platform at room temperature for 12 h, followed by a second wash at room temperture for 2 h. Slices were transferred to refractive index matching solution (RIMS) and incubated on an orbital shaker at room temperature for 2 h, then mounted on glass slides in

RIMS using 500-μm-thick spacers.

Immunohistochemistry: Animals were anesthetized and transcardially perfused with 4% paraformaldehyde. Brainstems were postfixed for 12 h at 4°C and sliced to a thickness of 30 μm, then permeabilized in 1x PBS with 0.4% Triton X-100 (PBS-T) for 30 min on a rotating platform at room temperature. Slices were incubated in 10% normal donkey serum (NDS) PBS-T blocking solution for 1 h on a rotating platform at room temperature. Following blocking, slices were incubated in primary antibody for NeuN (1:1000, MAB377, EMD Millipore; Billerica, MA) and SOX9 (1:500, AF3075, R&D Systems; Minneapolis, MN) diluted in PBS-T with 2.5% NDS on a rotating platform overnight at 4°C. Three 15-min washes in 1x PBS were performed, and then slices were incubated in secondary antibody (Donkey anti-rabbit IgG; 1:400, Abcam ab150073) conjugated to Alexa Fluor 488 in PBS-T for 2 h on a rotating platform at room temperature. Slices were wet mounted onto slides using aqueous, hard mount Vectashield (Vector Laboratories, Burlingame, CA).

Imaging and analysis: Specimens were examined with a Nikon A1 laser-scanning confocal microscope (Nikon; Melville, NY). Image stacks were acquired with a 40x, 1.15 NA water-immersion objective at a resolution of 350 x 350 μm at 1-μm intervals along the z-axis to a depth of 100 μm. FIJI software (Schindelin et al., 2012) was used to analyze morphologies and count neurons and glia. Circularity was computed in FIJI using the formula $4\pi*area/perimeter^2$

(a value of 1.0 indicates a perfect circle). Statistical hypothesis testing was performed using SPSS software (IBM; Armonk, NY). All measurements are reported as mean ± SD.

1.4 Results

Crossing $Dbx1^{+/CreERT2}$ heterozygotes with $Rosa26^{tdTomato}$ homozygotes yields litters that consist of roughly half mutant and half wild-type pups. To maximize the number of offspring carrying the Cre-ERT2 transgene, and thus eliminate the need to screen litters for tdTomato expression, we generated homozygous $Dbx1^{CreERT2}$ mice by interbreeding five pairs of $Dbx1^{+/CreERT2}$ heterozygotes and genotyping their offspring (n=69) using a probe for Cre recombinase. The histogram of the Cre signal showed a clear null column (n=19) and the remaining distribution was bimodal, with signals clustered in the 0.5-1.0 a.u. range (n=39) and the 1.5-2.0 a.u. range (n=11) (Fig. 1.1). We surmised that these clusters represented wild type, heterozygous, and homozygous $Dbx1^{CreERT2}$ mice, respectively. When we test crossed the putative homozygous $Dbx1^{CreERT2}$ mice with $Rosa26^{tdTomato}$ mice (which were homozygous from JAX), all of their offspring expressed tdTomato, as expected for a homozygous Cre-driver line. We observed no decrease in viability or fertility of the homozygous $Dbx1^{CreERT2}$ mice, which we then used to establish a colony.

First, to characterize the morphological properties of Dbx1-derived preBötC cells, we crossed $Dbx1^{CreERT2}$ mice with $Rosa26^{tdTomato}$ mice, administered
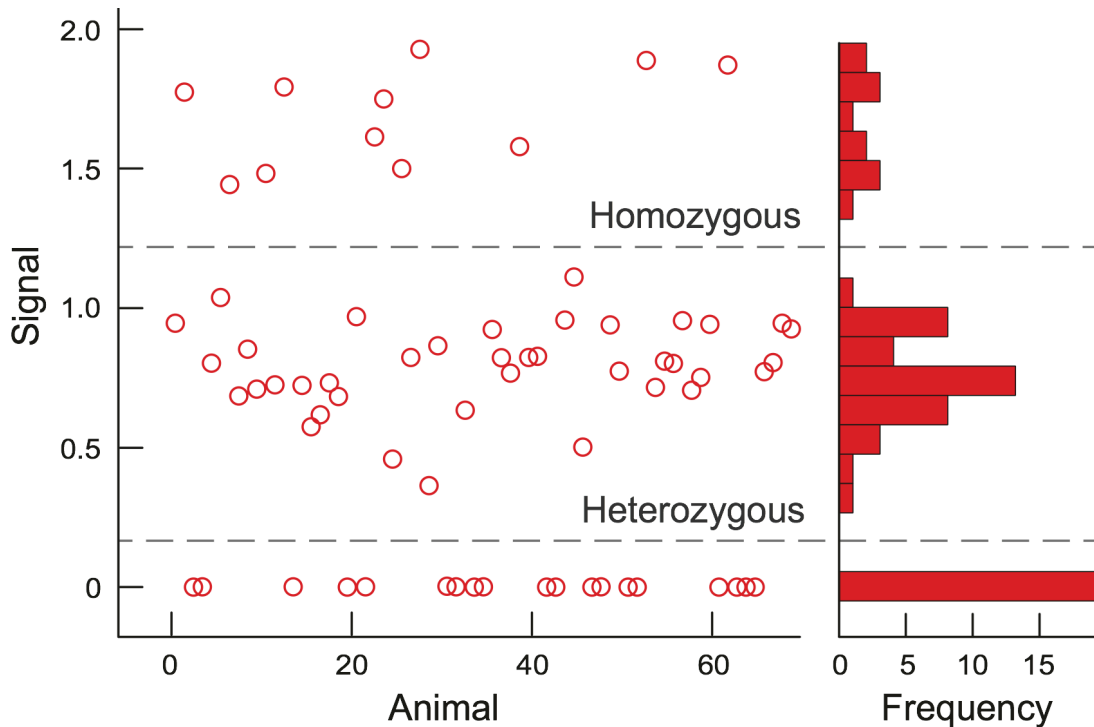
Figure 1.1. Generating homozygous $Dbx1^{CreERT2}$ mice. Tail clippings from the offspring (n=69) of five heterozygous $Dbx1^{+/CreERT2}$ breeding pairs were genotyped. Signal value was calculated by normalizing raw RT-PCR data for a Cre recombinase probe to a single copy housekeeping gene (*c-jun*) for each sample. Signal (in arbitrary units, a.u.) is plotted for each animal subject (left). The frequency histogram (right) has a bin size of 0.1 a.u. Samples can be interpreted as either wild type (no signal group, n=19), heterozygous (half-maximum signal group, n=39), or homozygous (maximum signal group, n=11).

tamoxifen to pregnant dams at E10.5, and screened their offspring (aged 6-8 weeks) for neuronal and glial markers. Three days after $Dbx1^{CreERT2}$; $Rosa26^{tdTomato}$ mice were injected with AAV-hSyn-GFP, we identified Dbx1-derived neurons based on cytosolic tdTomato and GFP expression (Fig. 1.2A). Alternatively, in $Dbx1^{CreERT2}$; $Rosa26^{tdTomato}$ mice not injected with AAV-hSyn-GFP, we identified Dbx1-derived neurons based on cytosolic tdTomato and nuclear NeuN expression (Fig. 1.2B). We inferred that cells with diffuse fibrils,

whose soma appeared smaller and more circular than NeuN-immunoreactive and GFP-expressing neurons, were glia. These putative Dbx1-derived glia expressed tdTomato but not GFP in animals injected with AAV-hSyn-GFP (Fig. 1.2A). Further, putative glia did not stain for NeuN (Fig. 1.2B) but were immunoreactive for the astrocyte marker Sox9 (Fig. 1.2C).

The somata of neurons (soma area = 389 ± 102 μm^2, n = 37) were larger than those of glia (soma area = 88 ± 22 μm^2, n = 34, unpaired t test, p < 0.0001, Fig. 1.2D). However, glial somata scored higher on circularity than neuronal somata (0.88 ± 0.05 versus 0.73 ± 0.09, unpaired t test, p < 0.0001, Fig. 1.2E). Neurons had fewer primary processes than glia (3-5 in neurons compared to 6-8 in glia), but the neuronal processes were notably thicker (diameter of ~1 μm in neurons versus ~200 nm in glia). The number and diameter of primary processes measured here in juvenile Dbx1 preBötC neurons match those of preBötC interneurons studied perinatally (Picardo et al., 2013). The round somata and the highly branched fibrils we observed in preBötC glia are characteristic of protoplasmic astrocytes, which could explain their Sox9 immunoreactivity (Stolt et al., 2003; Rowitch and Kriegstein, 2010; Robel et al., 2011).

Next, we aimed to identify the relationship between tamoxifen administration and tdTomato expression. We crossed $Dbx1^{CreERT2}$ females with $Rosa26^{tdTomato}$ males and administered tamoxifen via oral gavage to pregnant dams at embryonic days 7.5, 8.5, 9.5, 10.5, or 11.5 (E 7.5-11.5). For comparison, we
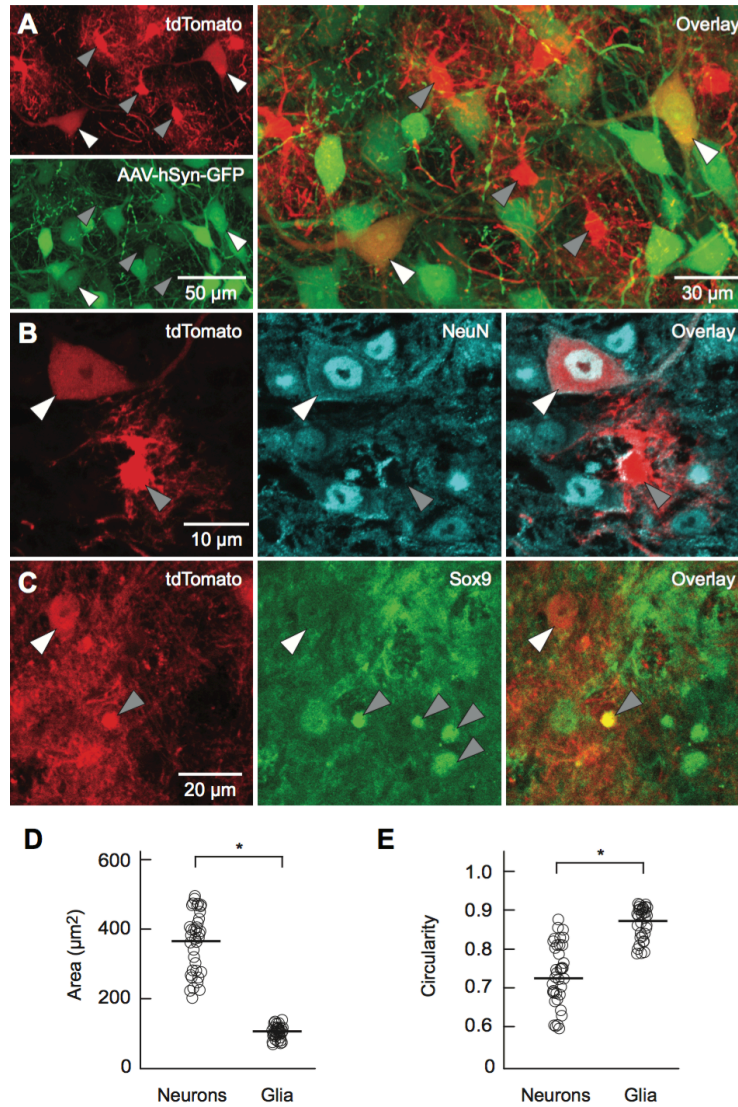
Figure 1.2. Dbx1-derived progenitors give rise to preBötC neurons and glia. *A*, Confocal images of *Dbx1*^{CreERT2}; *Rosa26*^{tdTomato} mouse preBötC sections 72 h after injection with AAV-hSyn-GFP. Dbx1-derived cells expressed native tdTomato fluorescence. Dbx1-derived neurons (white arrowheads) co-expressed tdTomato and GFP. Dbx1-derived glia (gray arrowheads) only expressed tdTomato. *B*, Confocal images of *Dbx1*^{CreERT2}; *Rosa26*^{tdTomato} mouse preBötC sections immunostained for NeuN. Dbx1-derived neurons (white arrowhead) expressed tdTomato and were immunoreactive for NeuN. Dbx1-derived glia (gray arrowhead) expressed tdTomato and were not immunoreactive for NeuN. *C*, Confocal images of *Dbx1*^{CreERT2}; *Rosa26*^{tdTomato} mouse preBötC sections immunostained for Sox9. Glia (gray arrowheads) were immunoreactive for Sox9. Dbx1-derived neurons (white arrowhead) expressed tdTomato but were not immunoreactive for Sox9. Dbx1-derived glia expressed tdTomato and were immunoreactive for Sox9 (see 'overlay' panel). *D*, Cross-sectional area of Dbx1-derived neurons and glia in the preBötC. *E*, Circularity score of Dbx1-derived neurons and glia in the preBötC. Asterisks in D and E signify p<0.0001).

crossed constitutive $Dbx1^{Cre}$ females with $Rosa26^{tdTomato}$ males, whose offspring express tdTomato in all Dbx1-derived cells. We performed the passive CLARITY technique on 500-µm-thick transverse brainstem slices from 6-8 week old offspring, and acquired confocal images (350 x 350 µm) of the preBötC to a depth of 100 µm.

TdTomato expression was widespread in $Dbx1^{Cre}$; $Rosa26^{tdTomato}$ sections. Labeled somata were densest in the dorsal region of the brainstem, lateral to the hypoglossal motor nucleus, and in wide (400-500 µm) bands extending dorsomedially from the hypoglossal motor nucleus to the ventrolateral edge of the brainstem (Fig. 1.3A, left). Although hypoglossal motor neurons did not express tdTomato, neuropil labeling occurred within the hypoglossal motor nucleus, as previously shown using $Dbx1^{CreERT2}$ mice (Ruangkittisakul et al., 2014). Neuropil was also densely labeled in the preBötC (Fig. 1.3A, middle). Based on morphological criteria from Fig. 1.2, we counted 70 ± 1 tdTomato-labeled neurons and 92 ± 4 tdTomato-labeled glia within the designated 350 x 350 x 100 µm imaging volume from the core of the preBötC (n = 2 cleared slices; Fig.1. 3A, right; Fig. 1.4).

In $Dbx1^{CreERT2}$; $Rosa26^{tdTomato}$ offspring, when tamoxifen was administered to pregnant dams at E7.5, tdTomato expression was diffuse and occurred mostly in somata dorsal and lateral to the hypoglossal motor nucleus (Fig. 1.3B, left). Neuropil labeling was sparse within the preBötC (particularly compared to the
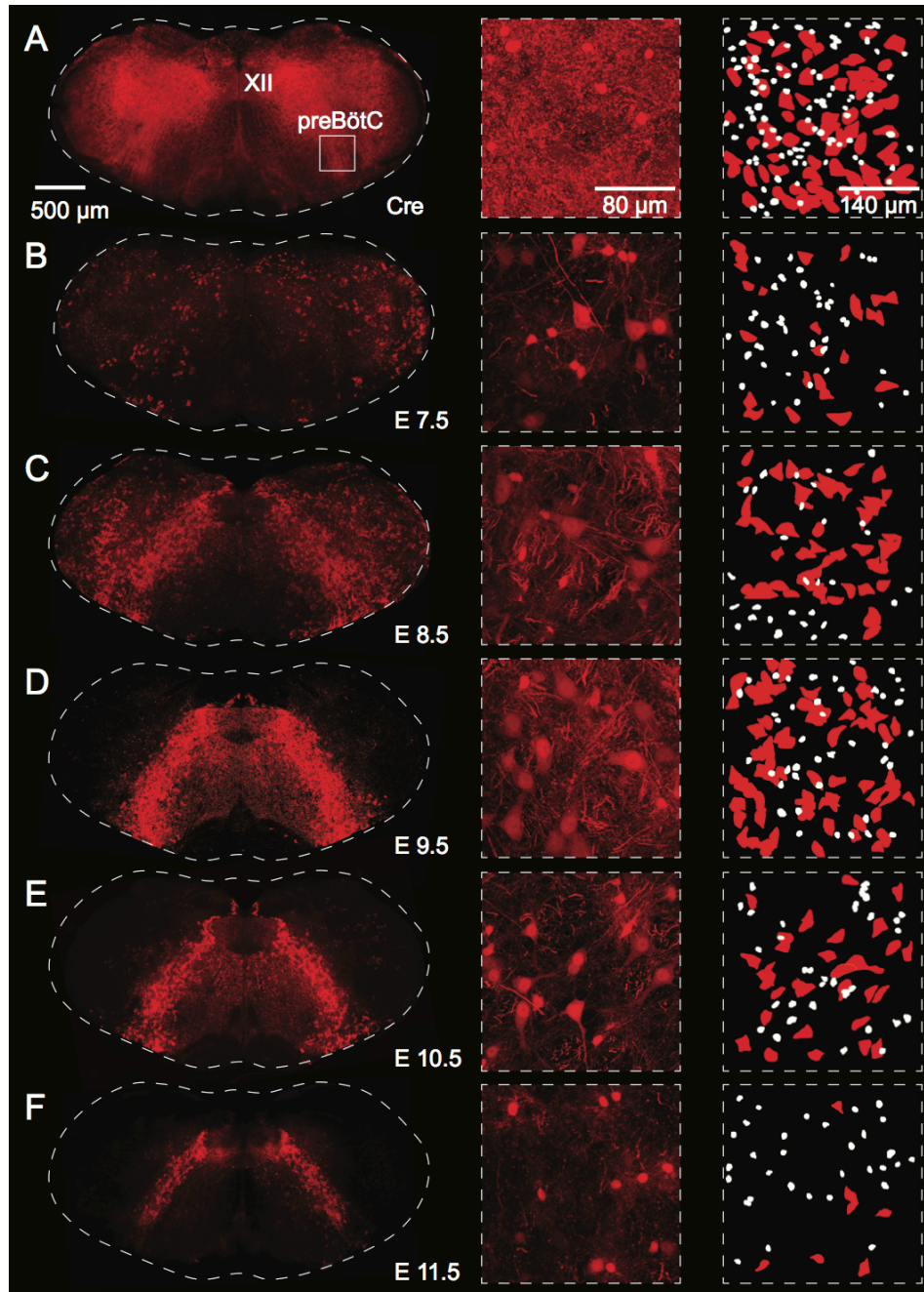
Figure 1.3. Relationship between tamoxifen timing and tdTomato expression. Left column: tdTomato expression in cleared mouse medullary preBötC sections from *Dbx1*[Cre]; *Rosa26*[tdTomato] mice (*A*) or *Dbx1*[CreERT2]; *Rosa26*[tdTomato] mice when tamoxifen was administered at E7.5-11.5 (*B-F*). Middle column: Confocal images (20-μm-thick z-projections) of the preBötC in *Dbx1*[Cre]; *Rosa26*[tdTomato] mice (*A*) or *Dbx1*[CreERT2]; *Rosa26*[tdTomato] mice (*B-F*). Right column: Masks of differentiated neurons (red) and glia (white) from 100-μm-thick z-projections in *Dbx1*[Cre]; *Rosa26*[tdTomato] mice (*A*) or *Dbx1*[CreERT2]; *Rosa26*[tdTomato] mice (*B-F*).

19

Dbx1[Cre]; *Rosa26*[tdTomato] mouse tissue), which improved our ability to distinguish individual cells (Fig. 1.3B, middle). We counted 23 ± 1 tdTomato-labeled neurons and 47 ± 7 tdTomato-labeled glia, which reflects 34% and 52% of the total number Dbx1-derived neurons and glia found, respectively, in the *Dbx1*[Cre]; *Rosa26*[tdTomato] mouse tissue (n = 3 cleared slices; Fig. 1.3B, right; Fig. 1.4).

In addition to diffuse labeling in dorsal and lateral brainstem regions, an inverted U-shaped expression pattern that was anchored at the ventrolateral edge of the brainstem and extended dorsomedially to the hypoglossal motor nucleus became visible when tamoxifen was administered to pregnant dams at E8.5 (Fig. 1.3C, left). The density of neuropil labeling increased in the preBötC but individual somata remained discernable (Fig. 1.3C, middle). We counted 38 ± 7 tdTomato-labeled neurons and 30 ± 6 tdTomato-labeled glia, which reflects 55% and 33% of the total number of Dbx1-derived neurons and glia found, respectively, in the *Dbx1*[Cre]; *Rosa26*[tdTomato] mouse tissue (n = 3 cleared slices; Fig. 1.3C, right; Fig. 1.4).

When tamoxifen was administered to pregnant dams at E9.5, the majority of tdTomato-labeled somata were confined to bands extending from the hypoglossal motor nucleus to the ventrolateral edges of the brainstem (Fig. 1.3D, left). Dense neuropil labeling was visible in the hypoglossal motor nucleus (also see Fig. 7 in Ruangkittisakul et al., 2014) similar to the offspring of *Dbx1*[Cre] mice (e.g., Fig 1.3A, left). Labeling of the neuropil and somata in the preBötC

was densest when tamoxifen was administered to pregnant dams at E9.5, but the magnitude was less than that of $Dbx1^{Cre}$; $Rosa26^{tdTomato}$ mice (compare Fig. 1.3D to 1.3A). We counted 63 ± 4 tdTomato-labeled neurons and 42 ± 1 tdTomato-labeled glia in the preBötC, which reflects 91% and 46% of the total number of Dbx1-derived neurons and glia found, respectively, in the $Dbx1^{Cre}$; $Rosa26^{tdTomato}$ mouse tissue (n = 3 cleared slices; Fig. 1.3D, right; Fig. 1.4).
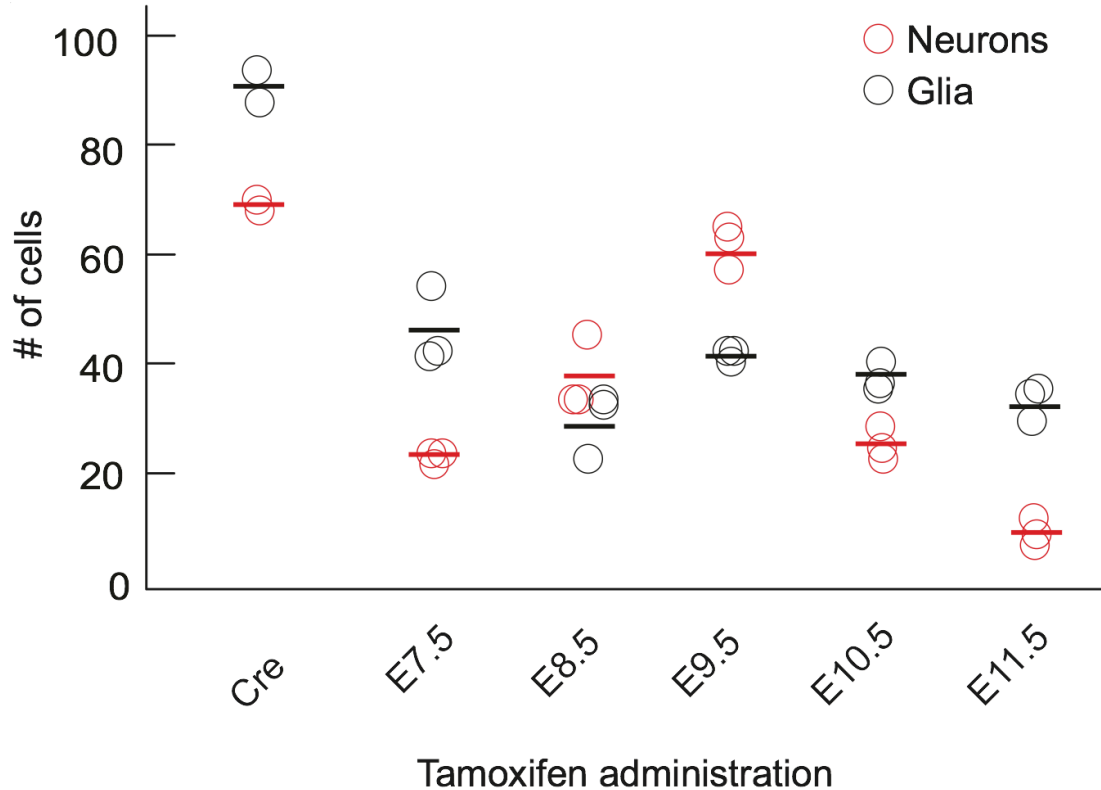
Figure 1.4. Quantifying preBötC neurons and glia as a function of tamoxifen administration timing. The ordinate plots the number of preBötC neurons (red circles) and glia (black circles) in our test volume of 350 x 350 x 100 µm on one side of the core of the preBötC in either $Dbx1^{Cre}$; $Rosa26^{tdTomato}$ mice (marked 'Cre' on the abscissa) or in $Dbx1^{CreERT2}$; $Rosa26^{tdTomato}$ mice, which are marked by when tamoxifen was administered to pregnant dams during embryonic development (E7.5-11.5). Each circle represents a single animal.

When tamoxifen was administered to pregnant dams at E10.5, tdTomato-labeled somata were more tightly confined to ~200-µm-wide bands extending dorsomedially from the hypoglossal motor nucleus to the ventrolateral edges of the brainstem (Fig. 1.3E, left). Labeling of neuropil in the medial region of the slice, between the U-shaped bands, as well as in the hypoglossal motor nucleus and preBötC, dwindled compared to the offspring of dams who received tamoxifen at E9.5 (compare Fig. 1.3E to 1.3D). We counted 26 ± 3 tdTomato-labeled neurons and 38 ± 3 tdTomato-labeled glia in the preBötC, which reflects 37% and 40% of the total number of Dbx1-derived neurons and glia found, respectively, in the *Dbx1*^Cre; *Rosa26*^tdTomato mouse tissue (n = 3 cleared slices; Fig 1.3E, right; Fig. 1.4).

When tamoxifen was administered at E11.5, tdTomato-labeled somata were tightly confined to bands extending from the hypoglossal motor nucleus and terminating in the preBötC (Fig. 1.3F, left). The bands were less prominent than in the offspring of dams who received tamoxifen between E8.5 and E10.5, and did not reach the ventral border. Neuropil was sparsely labeled in the hypoglossal motor nucleus and in the preBötC (Fig. 1.3F, middle). We counted 9 ± 3 tdTomato-labeled neurons and 34 ± 3 tdTomato-labeled glia, which reflects 14% and 36% of the total number of Dbx1-derived neurons and glia found, respectively, in the *Dbx1*^Cre; *Rosa26*^tdTomato mouse tissue (n = 3 cleared slices; Fig 1.3F, right; Fig. 1.4).

1.5 Discussion

Here we describe how tamoxifen administration timing in pregnant $Dbx1^{CreERT2}$ mice, crossed with an appropriate Cre-responder line, influences reporter protein expression in the preBötC of their offspring. Using homozygous $Dbx1^{CreERT2}$ mice, we show that Dbx1-derived progenitors give rise to morphologically distinct preBötC neurons and glia. Furthermore, we fate-map Dbx1-expressing progenitors by administering tamoxifen at different times during development, then quantify their progeny (as either neurons or glia) in the preBötC of juvenile mice. These data demonstrate the total number, as well as the relative proportion, of Dbx1-derived preBötC neurons and glia that expressthe reporter protein as a function of the timing of tamoxifen administration during embryogenesis. Peak neuronal reporter expression occurs when tamoxifen is administered at E9.5, but there is no relationship between tamoxifen timing and glial reporter expression.

We observed tdTomato expression in two morphologically distinct Dbx1-derived cell types, which we postulate to be neurons and glia. The cell bodies of putative glia are significantly smaller and more circular than neurons, and their primary processes are thinner and more sparsely branched. To ensure that we could reliably distinguish neurons from glia based on morphology, we probed the two populations for genetic and molecular markers. Using our morphological criteria to initially classify cells as either neurons or glia, we found that putative

glia do not express GFP driven by a synapsin promoter, and are not immunoreactive for NeuN. In addition, we found that putative neurons always expressed both markers. These data suggest that hindbrain Dbx1 proliferative zones generate preBötC neurons and glia that can be distinguished morphologically.

Classifying glia is challenging because there are several subtypes, for which few (if any) subtype-specific molecular markers are currently available. We found that nearly one third of Dbx1-derived preBötC glia were immunoreactive for Sox9, which suggests that they might be protoplasmic astrocytes. This is consistent with Gray et al. (2010), who showed that a subset of Dbx1-derived preBötC cells are immunoreactive for the astrocyte marker S100β. Notwithstanding, Sox9 and S100β have also been implicated in oligodendrocyte development (Stolt et al., 2003), and not all astrocytes express either marker. Oligodendrocytes, which are morphologically diverse, in some circumstances resemble the Dbx1-derived preBötC glia (e.g., compare our Fig. 1.2A,B to Fig. 3G in Zhao et al., 2016). Furthermore, Dbx1-expressing precursors of the ventricular zone give rise to a subpopulation of oligodendrocytes in the dorsal spinal cord (Fogarty et al., 2005), so it would not be surprising that Dbx1 also gives rise to oligodendrocytes in the hindbrain. Dbx1-derived preBötC glia likely include both astrocytes and oligodendrocytes, but their glial identities remain to be confirmed via definitive molecular markers.

Why is it significant that Dbx1-derived preBötC glia express the reporter protein? Studies investigating the origins of respiratory rhythmogenesis typically focus on neuronal mechanisms. However, astrocytes are chemosensitive and release ATP in response to hypoxia-induced intracellular Ca^{2+} elevations (Angelova et al., 2015). As a result, medullary astrocytes have been implicated in central chemoreception and respiratory control (Gourine et al., 2005; Funk et al., 2015). Further, preBötC astrocytes exhibit rhythmic Ca^{2+} elevations preceding inspiratory neuronal activity, and elicit single or burst firing of action potentials in inspiratory neurons when optogenetically stimulated (Okada et al., 2012). Because Dbx1-derived preBötC glia might influence respiratory rhythm, their physiological impact in experiments that utilize Dbx1-Cre driver mice must be considered. For example, Cre-driver mice crossed with Cre-dependent channelrhodopsin reporters enable photo-activation of Dbx1 preBötC neurons (Kottick and Del Negro, 2015; Anderson et al., 2016; Cui et al., 2016). It is reasonable to assume that Dbx1-derived glia also expressed channelrhodopsin, and were also photo-activated in parallel with Dbx1 neurons. Similarly, Cre-driver mice have been crossed with Cre-dependent archaerhodopsin reporters to transiently suppress Dbx1 preBötC neurons. (Koizumi et al., 2016; Vann et al., 2016). In some systems, mastication for example, astrocytes appear to play an integral role in rhythm and burst generation (Morquette et al., 2015). However, for respiratory rhythm in the preBötC, the role(s) of astrocytes are far from clear at this stage.

Although it is unclear how transient activation or suppression of preBötC glia might impact the results of these experiments, our data suggest that any confounding influence of reporter-expressing glia can be strategically mitigated in future neurophysiology studies. To minimize reporter protein expression in glia, the breeding and tamoxifen administration strategy can bias reporter protein expression towards neurons. We found that when tamoxifen is administered at E9.5, $Dbx1^{CreERT2}$; $Rosa26^{tdTomato}$ mice express tdTomato in 91% of the total neurons that express tdTomato in $Dbx1^{Cre}$; $Rosa26^{tdTomato}$ mice, but only 46% as many glia. Further, the density of tdTomato expressing neuropil in the preBötC of $Dbx1^{CreERT2}$; $Rosa26^{tdTomato}$ mice is lower than in their $Dbx1^{Cre}$; $Rosa26^{tdTomato}$ counterparts. This facilitates identification of Dbx1-derived neuronal somata based on morphology. To minimize the influence of glia in physiological experiments aimed at manipulating the activity of Dbx1 neurons, we advocate using $Dbx1^{CreERT2}$ mice (in which tamoxifen administration occurs at E9.5) as opposed to $Dbx1^{Cre}$ mice. We also recommend using $Dbx1^{CreERT2}$ mice for targeted recordings or ablations, because the low background fluorescence will aid in accurate visual identification of Dbx1 cells.

Because Cre-mediated recombination does not occur in all Dbx1-derived cells in $Dbx1^{CreERT2}$; Cre-dependent reporter crosses, we recommend using constitutive $Dbx1^{Cre}$ mice for experiments that cannot tolerate false-negatives (i.e., cells that do not express reporter protein, but are Dbx1-derived). For

example, *Dbx1*^{Cre} mice should be used for experiments that involve electrophysiological, RT-PCR, or RNA-Seq comparisons of Dbx1- and non-Dbx1-derived preBötC cells, or any experiment that involves identifying non-Dbx1 cells based on lack of reporter protein expression.

These data can also be used to devise strategies to address the role of Dbx1-derived glia in respiratory rhythm generation. Crossing *Dbx1*^{CreERT2}; *Rosa26*^{tdTomato} mice and administering tamoxifen at E7.5 or E11.5 sparsely labels neuropil in the preBötC and yet labels twice as many glia as neurons. Under these circumstances, detailed morphologies of glia can be acquired, and glia would be easy to distinguish for targeted electrophysiological recordings or calcium imaging. One could ablate Dbx1-derived astrocytes by crossing constitutive *Dbx1*^{Cre} mice with Aldh1L1-eGFP-Stop-DTA mice (Tsai et al., 2012; stock no. 026033, Jackson Laboratory), which would activate Diphtheria toxin expression in (and subsequently destroy) Aldh1l1-expressing Dbx1-derived astrocytes. However, this experiment would destroy all Dbx1-derived Aldh1l1-expressing cells, including those outside of the preBötC. We are not currently aware of any available transgenic strains that would permit targeted manipulation of Dbx1-derived preBötC glia, but it might involve crossing Dbx1-Cre driver mice with Cre-dependent reporters whose genomes have been modified to express a light gated ion channel or proton pump under the control of a glia-specific promoter.

Dbx1 preBötC neurons have respiratory rhythm-generating and premotor function (Bouvier et al., 2010; Gray et al., 2010), and represent a therapeutic target for respiratory related pathologies like opioid-induced respiratory depression, sleep apnea, and cell-death due to aging or neurodegenerative disease. Therefore, it is physiologically relevant to determine the anatomical boundaries of the preBötC and quantify its constituent interneurons. Studies of rhythmically-active brainstem preparations suggest that the preBötC extends along the rostral-caudal axis for ~150 µm in neonatal mice (Ruangkittisakul et al., 2011, 2014) and ~200 µm in neonatal rats (Ruangkittisakul et al., 2006, 2008). It is centered at the level of the subcompact nucleus ambiguus, where the principal loop of the inferior olive is fully developed and the medial inferior olive shows a sharp dorsomedial "stalk-like" appearance. Histological analysis of these landmarks in three-month-old mice suggests that the preBötC spans 440 µm in the rostral-caudal axis in juveniles (similar to the mice used in this study) (Franklin and Paxinos, 2013). In the transverse plane, the dorsal border of the preBötC is located ventral to the nucleus ambiguus and its ventral border is parallel to the dorsal boundary of the inferior olive (Gray et al., 2001; Ruangkittisakul et al., 2006, 2008, 2011, 2014), a region spanning roughly 350 x 350 µm in our brainstem sections (Fig. 1.3). Based on these anatomical studies, we estimate the preBötC to occupy a volume of 350 x 350 x 440 µm in our $Dbx1^{Cre}$; $Rosa26^{tdTomato}$ mice. We identified ~70 neurons in a 350 x 350 x 100 µm region in the center of the preBötC. Extrapolating these data to match

the dimensions of the preBötC provides an estimate of 616 Dbx1-derived preBötC neurons. This enumeration is similar to other estimates of the essential preBötC core containing ~550 neurons in neonatal mice (Wang et al., 2014) and ~600 neurons in adult rats (Gray et al., 2001). We therefore conclude that ~600 neurons is a reasonable estimate for the size of the network comprising the rhythmogenic core of the preBötC in mice.

This study describes the developmental assemblage of the preBötC, both its neuronal and glial components. These findings can be used to bias reporter protein expression towards preBötC neurons (or could be applied to investigate the respiratory role(s) of Dbx1-derived glia). By optimizing this tool, we can design better experiments to interrogate the mechanisms underlying respiratory rhythmogenesis and pattern formation.

1.6 References

Anderson TM, Garcia AJ, Baertsch NA, Pollak J, Bloom JC, Wei AD, Rai KG, Ramirez J-M (2016) A novel excitatory network for the control of breathing. Nature 536:76–80.

Angelova PR, Kasymov V, Christie I, Sheikhbahaei S, Turovsky E, Marina N, Korsak A, Zwicker J, Teschemacher AG, Ackland GL, Funk GD, Kasparov S, Abramov AY, Gourine AV (2015) Functional Oxygen Sensitivity of Astrocytes. J Neurosci Off J Soc Neurosci 35:10460–10473.

Bielle F, Griveau A, Narboux-Nême N, Vigneau S, Sigrist M, Arber S, Wassef M, Pierani A (2005) Multiple origins of Cajal-Retzius cells at the borders of

the developing pallium. Nat Neurosci 8:1002–1012.

Bouvier J, Thoby-Brisson M, Renier N, Dubreuil V, Ericson J, Champagnat J, Pierani A, Chédotal A, Fortin G (2010) Hindbrain interneurons and axon guidance signaling critical for breathing. Nat Neurosci 13:1066–1074.

Cui Y, Kam K, Sherman D, Janczewski WA, Zheng Y, Feldman JL (2016) Defining preBötzinger Complex Rhythm- and Pattern-Generating Neural Microcircuits In Vivo. Neuron 91:602–614.

Feldman JL, Del Negro CA, Gray PA (2013) Understanding the rhythm of breathing: so near, yet so far. Annu Rev Physiol 75:423–452.

Fogarty M, Richardson WD, Kessaris N (2005) A subset of oligodendrocytes generated from radial glia in the dorsal spinal cord. Dev Camb Engl 132:1951–1959.

Franklin K, Paxinos G (2013) Paxinos and Franklin's the mouse brain in stereotaxic coordinates. Fourth edition. Academic Press, an imprint of Elsevier.

Funk GD, Rajani V, Alvares TS, Revill AL, Zhang Y, Chu NY, Biancardi V, Linhares-Taxini C, Katzell A, Reklow R (2015) Neuroglia and their roles in central respiratory control; an overview. Comp Biochem Physiol A Mol Integr Physiol 186:83–95.

Gourine AV, Llaudet E, Dale N, Spyer KM (2005) ATP is a mediator of chemosensory transduction in the central nervous system. Nature 436:108–111.

Gray PA, Hayes JA, Ling GY, Llona I, Tupal S, Picardo MCD, Ross SE, Hirata T, Corbin JG, Eugenín J, Del Negro CA (2010) Developmental origin of

preBötzinger complex respiratory neurons. J Neurosci Off J Soc Neurosci 30:14883–14895.

Gray PA, Janczewski WA, Mellen N, McCrimmon DR, Feldman JL (2001) Normal breathing requires preBötzinger complex neurokinin-1 receptor-expressing neurons. Nat Neurosci 4:927–930.

Hirata T, Li P, Lanuza GM, Cocas LA, Huntsman MM, Corbin JG (2009) Identification of distinct telencephalic progenitor pools for neuronal diversity in the amygdala. Nat Neurosci 12:141–149.

Koizumi H, Mosher B, Tariq MF, Zhang R, Koshiya N, Smith JC (2016) Voltage-Dependent Rhythmogenic Property of Respiratory Pre-Bötzinger Complex Glutamatergic, Dbx1-Derived, and Somatostatin-Expressing Neuron Populations Revealed by Graded Optogenetic Inhibition. eNeuro 3.

Kottick A, Del Negro CA (2015) Synaptic Depression Influences Inspiratory-Expiratory Phase Transition in Dbx1 Interneurons of the preBötzinger Complex in Neonatal Mice. J Neurosci Off J Soc Neurosci 35:11606–11611.

Moore JD, Deschênes M, Furuta T, Huber D, Smear MC, Demers M, Kleinfeld D (2013) Hierarchy of orofacial rhythms revealed through whisking and breathing. Nature 497:205–210.

Morquette P, Verdier D, Kadala A, Féthière J, Philippe AG, Robitaille R, Kolta A (2015) An astrocyte-dependent mechanism for neuronal rhythmogenesis. Nat Neurosci 18:844–854.

Okada Y, Sasaki T, Oku Y, Takahashi N, Seki M, Ujita S, Tanaka KF, Matsuki N, Ikegaya Y (2012) Preinspiratory calcium rise in putative pre-Botzinger

complex astrocytes. J Physiol 590:4933–4944.

Picardo MCD, Weragalaarachchi KTH, Akins VT, Del Negro CA (2013) Physiological and morphological properties of Dbx1-derived respiratory neurons in the pre-Botzinger complex of neonatal mice. J Physiol 591:2687–2703.

Pierani A, Moran-Rivard L, Sunshine MJ, Littman DR, Goulding M, Jessell TM (2001) Control of interneuron fate in the developing spinal cord by the progenitor homeodomain protein Dbx1. Neuron 29:367–384.

Revill AL, Vann NC, Akins VT, Kottick A, Gray PA, Del Negro CA, Funk GD (2015) Dbx1 precursor cells are a source of inspiratory XII premotoneurons. eLife 4.

Robel S, Berninger B, Götz M (2011) The stem cell potential of glia: lessons from reactive gliosis. Nat Rev Neurosci 12:88–104.

Rowitch DH, Kriegstein AR (2010) Developmental genetics of vertebrate glial-cell specification. Nature 468:214–222.

Ruangkittisakul A, Kottick A, Picardo MCD, Ballanyi K, Del Negro CA (2014) Identification of the pre-Bötzinger complex inspiratory center in calibrated "sandwich" slices from newborn mice with fluorescent Dbx1 interneurons. Physiol Rep 2.

Ruangkittisakul A, Panaitescu B, Ballanyi K (2011) K(+) and Ca^2(+) dependence of inspiratory-related rhythm in novel "calibrated" mouse brainstem slices. Respir Physiol Neurobiol 175:37–48.

Ruangkittisakul A, Schwarzacher SW, Secchia L, Ma Y, Bobocea N, Poon BY, Funk GD, Ballanyi K (2008) Generation of eupnea and sighs by a

spatiochemically organized inspiratory network. J Neurosci Off J Soc Neurosci 28:2447–2458.

Ruangkittisakul A, Schwarzacher SW, Secchia L, Poon BY, Ma Y, Funk GD, Ballanyi K (2006) High sensitivity to neuromodulator-activated signaling pathways at physiological [K+] of confocally imaged respiratory center neurons in on-line-calibrated newborn rat brainstem slices. J Neurosci Off J Soc Neurosci 26:11870–11880.

Schindelin J, Arganda-Carreras I, Frise E, Kaynig V, Longair M, Pietzsch T, Preibisch S, Rueden C, Saalfeld S, Schmid B, Tinevez J-Y, White DJ, Hartenstein V, Eliceiri K, Tomancak P, Cardona A (2012) Fiji: an open-source platform for biological-image analysis. Nat Methods 9:676–682.

Smith JC, Ellenberger HH, Ballanyi K, Richter DW, Feldman JL (1991) Pre-Bötzinger complex: a brainstem region that may generate respiratory rhythm in mammals. Science 254:726–729.

Stolt CC, Lommes P, Sock E, Chaboissier M-C, Schedl A, Wegner M (2003) The Sox9 transcription factor determines glial fate choice in the developing spinal cord. Genes Dev 17:1677–1689.

Treweek JB, Chan KY, Flytzanis NC, Yang B, Deverman BE, Greenbaum A, Lignell A, Xiao C, Cai L, Ladinsky MS, Bjorkman PJ, Fowlkes CC, Gradinaru V (2015) Whole-body tissue stabilization and selective extractions via tissue-hydrogel hybrids for high-resolution intact circuit mapping and phenotyping. Nat Protoc 10:1860–1896.

Tsai H-H, Li H, Fuentealba LC, Molofsky AV, Taveira-Marques R, Zhuang H, Tenney A, Murnen AT, Fancy SPJ, Merkle F, Kessaris N, Alvarez-Buylla A, Richardson WD, Rowitch DH (2012) Regional astrocyte allocation regulates CNS synaptogenesis and repair. Science 337:358–362.

Vann NC, Pham FD, Hayes JA, Kottick A, Del Negro CA (2016) Transient Suppression of Dbx1 PreBötzinger Interneurons Disrupts Breathing in Adult Mice. PloS One 11:e0162418.

Wang X, Hayes JA, Revill AL, Song H, Kottick A, Vann NC, LaMar MD, Picardo MCD, Akins VT, Funk GD, Del Negro CA (2014) Laser ablation of Dbx1 neurons in the pre-Bötzinger complex stops inspiratory rhythm and impairs output in neonatal mice. eLife 3:e03427.

Zhao C, Deng Y, Liu L, Yu K, Zhang L, Wang H, He X, Wang J, Lu C, Wu LN, Weng Q, Mao M, Li J, van Es JH, Xin M, Parry L, Goldman SA, Clevers H, Lu QR (2016) Dual regulatory switch through interactions of Tcf7l2/Tcf4 with stage-specific partners propels oligodendroglial maturation. Nat Commun 7:10883.

CHAPTER 2: Synaptic depression influences inspiratory-expiratory phase transition in Dbx1 preBötzinger Complex interneurons in neonatal mice

2.1 Abstract

The brainstem preBötzinger Complex (preBötC) generates the rhythm underlying inspiratory breathing movements and its core interneurons are derived from *Dbx1*-expressing precursors. Recurrent synaptic excitation is required to initiate inspiratory bursts, but whether excitatory synaptic mechanisms also contribute to inspiratory-expiratory phase transition is unknown. Here we examined the role of short-term synaptic depression using a rhythmically active neonatal mouse brainstem slice preparation. We show that afferent axonal projections to Dbx1 preBötC neurons undergo activity-dependent depression, and we identify a refractory period (~2 s) following endogenous inspiratory bursts that precludes light-evoked bursts in channelrhodopsin-expressing Dbx1 preBötC neurons. We demonstrate that the duration of the refractory period – but neither the cycle period nor the magnitude of endogenous inspiratory bursts – is sensitive to changes in extracellular Ca^{2+}. Further, we show that postsynaptic factors are unlikely to explain the refractory period or its modulation by Ca^{2+}. Our findings are consistent with the hypothesis that short-term synaptic depression in Dbx1 preBötC neurons influences the inspiratory-expiratory phase transition during respiratory rhythmogenesis.

2.2 Introduction

Breathing movements emanate from neural rhythms in the preBötzinger Complex (preBötC) of the ventrolateral medulla (Smith et al., 1991; Feldman et al., 2013; Moore et al., 2013). The breathing cycle consists of an inspiratory phase wherein preBötC neurons discharge bursts of spikes synchronously followed by a two-part expiratory phase in which preBötC neurons remain quiescent at least during the initial post-inspiratory stage (but may recover spontaneous activity during the second expiratory stage). Core rhythm-generating preBötC interneurons are derived from progenitors that express the homeobox gene *Dbx1* (henceforth referred to as Dbx1 neurons), which are glutamatergic and interconnected bilaterally in the preBötC (Bouvier et al., 2010; Gray et al., 2010). AMPA receptor-mediated excitatory interactions are required to initiate inspiratory bursts (Funk et al., 1993; Wallén-Mackenzie et al., 2006), but there is no consensus regarding the cellular and synaptic mechanisms that terminate inspiratory bursts and lead to the quiescent post-inspiratory phase of respiratory cycle (i.e., inspiratory-expiratory phase transition).

A longstanding view posits that the inspiratory-expiratory phase transition depends on respiratory circuits throughout the pons and medulla operating via postsynaptic inhibition (Richter, 1982; Bianchi et al., 1995). However, the obligatory role of inhibition is falsified by experiments that block chloride-mediated synaptic transmission in respiratory networks but do not significantly

perturb respiratory rhythm *in vitro* (Brockhaus and Ballanyi, 1998; Ren and Greer, 2006; Feldman et al., 2013) or *in vivo* (Janczewski et al., 2013; Sherman et al., 2015). One alternative mechanism that does not depend on distributed inhibitory circuits is the *group pacemaker*, which instead focuses on collective activity among preBötC neurons. According to this model, recurrent excitatory synaptic activity initiates inspiratory bursts (for which there is strong evidence: Rekling and Feldman, 1998; Pace et al., 2007; Carroll and Ramirez, 2013; Carroll et al., 2013) and short-term synaptic depression promotes burst termination and inspiratory-expiratory phase transition (but this latter part remains an untested model prediction: Rubin et al., 2009).

Using the group-pacemaker model as our conceptual framework, we investigated the role of short-term synaptic depression in respiratory rhythm generation. Our results in a reduced slice context support the group-pacemaker model and are consistent with the notion that presynaptic depression in Dbx1 preBötC neurons facilitates inspiratory burst termination and influences post-inspiratory network activity.

2.3 Materials and Methods

The Institutional Animal Care and Use Committee at the College of William & Mary approved these protocols. We used female mice that express Cre recombinase fused to a tamoxifen-sensitive mutant form of the human estrogen receptor (CreERT2) in cells that express the *Dbx1* gene, *Dbx1^CreERT2^*. For

optical stimulation experiments, female Cre-driver mice were mated with male reporter mice whose *Rosa26* locus was modified by targeted insertion of a *loxP*-flanked STOP cassette followed by a *channelrhodopsin-tdTomato* fusion gene (*Rosa26$^{hChR2(H134R)-tdTomato}$*, stock no. 12567, Jackson Laboratory, Bar Harbor, ME). To record Dbx1 neurons, female Cre-driver mice were mated with male reporter mice that express Cre-dependent tdTomato (*Rosa26^{tdTomato}*, stock no. 007905, Jackson Laboratory). Tamoxifen (22.5 mg·kg^{-1} body mass) was administered to pregnant females at embryonic day 9.5. Cre-mediated recombination resulted in the expression of the hChR2-tdTomato or cytosolic tdTomato, in neurons whose progenitors express *Dbx1*.

We anesthetized neonatal mice via hypothermia and dissected their neuraxes in artificial cerebrospinal fluid (aCSF) containing (in mM): 124 NaCl, 3 KCl, 1.5 CaCl$_2$, 1 MgSO$_4$, 25 NaHCO$_3$, 0.5 NaH$_2$PO$_4$, and 30 dextrose equilibrated with 95% O$_2$/5% CO$_2$, pH: 7.4. This aCSF was varied in one set of experiments by substituting MgCl$_2$ for MgSO$_4$. Thus, changes in CaCl$_2$ were counterbalanced by MgCl$_2$ to maintain the net divalent cation concentration and Cl$^-$ gradient.

Transverse medullary slices (500 µm thick) that expose the preBötC rostrally (Ruangkittisakul et al., 2014) were perfused with 26°C aCSF at 5 ml·min^{-1}. Extracellular K$^+$ was elevated to 9 mM to sustain respiratory rhythm and motor output, which we recorded from hypoglossal (XII) nerve rootlets. XII discharge was amplified (2000x), band-pass filtered (300-1000 Hz), and then full-wave

rectified and smoothed for display.

We obtained whole-cell patch-clamp recordings under visual control using bright-field imaging on a fixed-stage microscope. Dbx1 neurons were identified by epifluorescence (Cy3 filter set). Patch pipettes (4-6 MΩ) were fabricated from capillary glass (1.50 mm outer diameter, 0.86 mm inner diameter). Patch pipette solution contained (in mM): 140 potassium gluconate, 5 NaCl, 0.1 EGTA, 10 HEPES, 2 Mg-ATP, 0.3 Na_3-GTP, and 50-µM Alexa 488 hydrazide dye (Invitrogen, Carlsbad, CA). Membrane potential was amplified (100x) and low-pass filtered (1 kHz) using a current-clamp amplifier before being digitally acquired at 10 kHz.

A glass micropipette connected to a stimulus isolation unit (3 µA for 5 ms) was used to stimulate midline-crossing axons. Evoked EPSPs with amplitudes that exceeded baseline potential fluctuations by >2 SD were considered for analysis. The preBötC contralateral to the whole-cell recording site was illuminated using a 100-µm diameter fiber coupled to a 100-mW 473-nm laser (IkeCool, Anaheim, CA). AMPA (100 µM, Sigma Aldrich, St Louis, MO) was applied to Dbx1 preBötC neurons using a patch pipette connected to a pressure ejection system (5 pulses at 5 psi for 5 ms each; Toohey Company, Fairfield, NJ). Midline electrical stimulations and AMPA application experiments were performed in 3 mM extracellular K^+ to decrease baseline membrane potential fluctuations and to minimize contributions from spontaneous EPSPs.

We measured the peak amplitude and area of inspiratory bursts in Dbx1 preBötC neurons by digitally smoothing the membrane potential trajectory to eliminate spikes but preserve the underlying envelope of depolarization. Ionotropic receptor antagonists were applied at these concentrations (in µM): 10 CNQX, 20 dl-APV, 5 picrotoxin (PTX), and 5 strychnine (STY) (Sigma).

We report all measurements as mean ± SD. SPSS software (IBM, Armonk, NY) compared group means and probability distributions for statistical hypothesis testing. Paired-sample t-tests evaluated mean differences between two groups and the Kolmogorov-Smirnov test compared cumulative probability distributions. Nonparametric Friedman tests evaluated mean differences in repeated measures experiments when data did not meet the assumptions of normality and homogeneity of variance required for parametric analysis.

2.4 Results

Dbx1 Cre-driver mice (*Dbx1*^{CreERT2}) were coupled with two different flox-stop reporter strains to selectively record and optically manipulate Dbx1 neurons in transverse brainstem slices that provide optimal experimental access to the preBötC. We identified Dbx1 neurons by native fluorescence in the region of the slice ventral to the semi-compact division of the nucleus ambiguus (scNA) and orthogonal to the dorsal boundary of the principal loop of the inferior olive (IO$_{loop}$), which corresponds to the rostral face of the preBötC (Fig. 2.1A) (Ruangkittisakul et al., 2014). Dbx1 preBötC neurons, dialyzed with Alexa 488

through the patch pipette (Fig. 2.1B), discharged inspiratory bursts in phase with inspiratory-related XII nerve output (Fig. 2.1C).
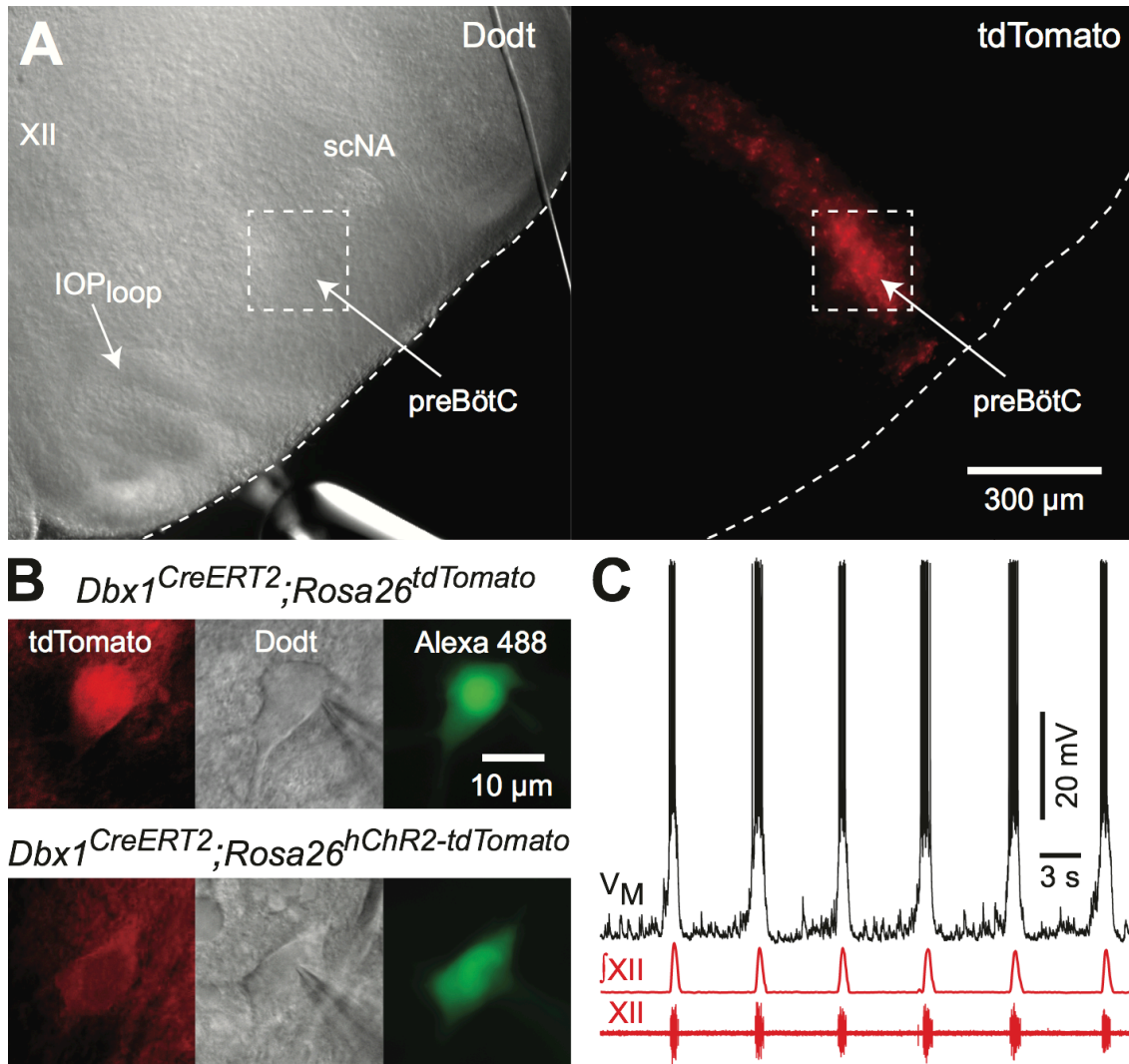
Figure 2.1. Rhythmically active slices expose Dbx1 preBötC neurons. A, Rostral slice surface from a *Dbx1^CreERT2^; Rosa26^tdTomato^* mouse pup showing hypoglossal motor nucleus (XII), semi-compact division of the nucleus ambiguus (scNA), and the principal loop of the inferior olive (IO_loop), sites co-localized with the preBötC (left). Dotted box marks the preBötC. B, Whole-cell recordings in *Dbx1^CreERT2^; Rosa26^tdTomato^* (top) and *Dbx1^CreERT2^; Rosa26^thChR2-tdTomato^* (bottom) mouse slices. tdTomato (left), Dodt contrast microscopy (middle), and Alexa 488 introduced via patch pipette (right). C, Inspiratory bursts in the Dbx1 preBötC neuron from B (top) with XII motor output.

Dbx1 preBötC interneurons project commissural axons to form synaptic connections with the contralateral preBötC (Bouvier et al., 2010). To determine if excitatory synapses onto Dbx1 preBötC neurons undergo activity-dependent depression, we repetitively stimulated commissural axons during whole-cell recordings in $Dbx1^{CreERT2};Rosa26^{tdTomato}$ mouse slices. We observed a progressive amplitude reduction of evoked EPSPs (Fig. 2.2A, n=8 Dbx1 neurons, 3 trials/neuron). Furthermore, the number of failures increased during each trial such that the last five pulses experienced a 40-50% failure rate (Fig. 2.2B). These data indicate that excitatory synapses among Dbx1 preBötC neurons undergo activity-dependent depression even when activated at a rate of 5 Hz, which is lower than typical intra-burst spike frequency of 15-50 Hz.

We reasoned that if short-term synaptic depression influences inspiratory-expiratory phase transition, then its effects would be measurable at the network level immediately after an endogenous inspiratory burst. First we tested whether inspiratory-like bursts could be triggered by light in $Dbx1^{CreERT2};Rosa26^{hChR-tdTomato}$ mouse slices. We evoked bursts using 100-ms pulses of blue light delivered to the preBötC contralateral to the whole-cell recording site. Evoked bursts were reversibly blocked by the AMPA receptor antagonist CNQX, but not by co-application of the NMDA receptor antagonist AP5 with the $GABA_A$ and glycine receptor antagonists picrotoxin and strychnine (Fig. 2.3A). These data demonstrate that evoked bursts depend on AMPA
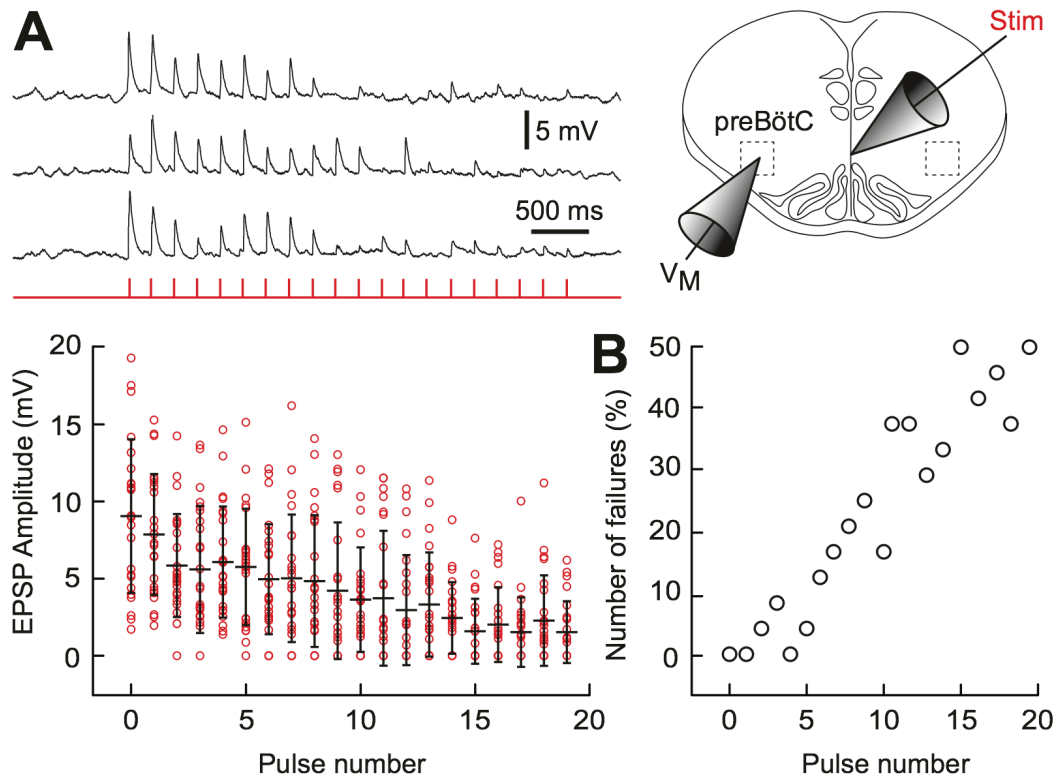
Figure 2.2. Activity-dependent synaptic depression in Dbx1 preBötC neurons. A, Evoked EPSPs in response to 5 Hz electrical stimulation of midline-crossing axons (top); group data from eight Dbx1 preBötC neurons (time synced) are shown below. Red circles show EPSP amplitudes; black bars show mean ± SD. B, relative frequency of failures to evoke an EPSP as a function of pulse number.

receptor-mediated synaptic interactions, akin to endogenous inspiratory bursts (Funk et al., 1993; Wallén-Mackenzie et al., 2006), whereas NMDA receptors and chloride-mediated inhibition are dispensable (Brockhaus and Ballanyi, 1998; Ren and Greer, 2006; Feldman et al., 2013; Janczewski et al., 2013; Sherman et al., 2015).

We applied transient light pulses at varying intervals after endogenous inspiratory bursts, which reliably evoked subsequent bursts for intervals >2 s.

However, intervals <2 s failed to evoke a burst (Fig. 2.3B). In this context, we defined the refractory period as the minimum duration after an endogenous inspiratory burst necessary to evoke a subsequent inspiratory-like burst whose amplitude was ≥75% of the average endogenous inspiratory burst (Fig. 2.3C). The refractory period duration was significantly shorter than the endogenous burst period (1.94 ± 0.74 s vs. 5.80 ± 1.49 s, n=10 preparations, Student's t(8)=7.62, p=5.6E-6). These data suggest that a ~2 s refractory period is a previously unrecognized component of the respiratory cycle in Dbx1 preBötC neurons. This refractory period is relevant during the post-inspiratory phase (~2 s in duration) but not the remaining 3-4 s of the expiratory phase *in vitro*.

Pre- and postsynaptic factors cause short-term synaptic depression. Both could potentially contribute to the refractory period (Fig. 2.3). First, we examined postsynaptic AMPA receptor desensitization as a potential contributing factor to the refractory period by comparing the amplitude of spontaneous EPSPs (sEPSPs) that were measurable before and after endogenous inspiratory bursts in Dbx1 preBötC neurons (Fig. 2.4A, left). We observed no difference in the cumulative probability sEPSP amplitude histogram (Fig. 2.4A, right, n=8 Dbx1 neurons, 10 cycles/neuron, Kolmogorov-Smirnov test statistic D=0.081, p=0.89), suggesting that AMPA receptors do not remain desensitized for seconds after endogenous inspiratory bursts and therefore do not contribute to the refractory period. Nevertheless, it is conceivable that the sEPSPs we measured might
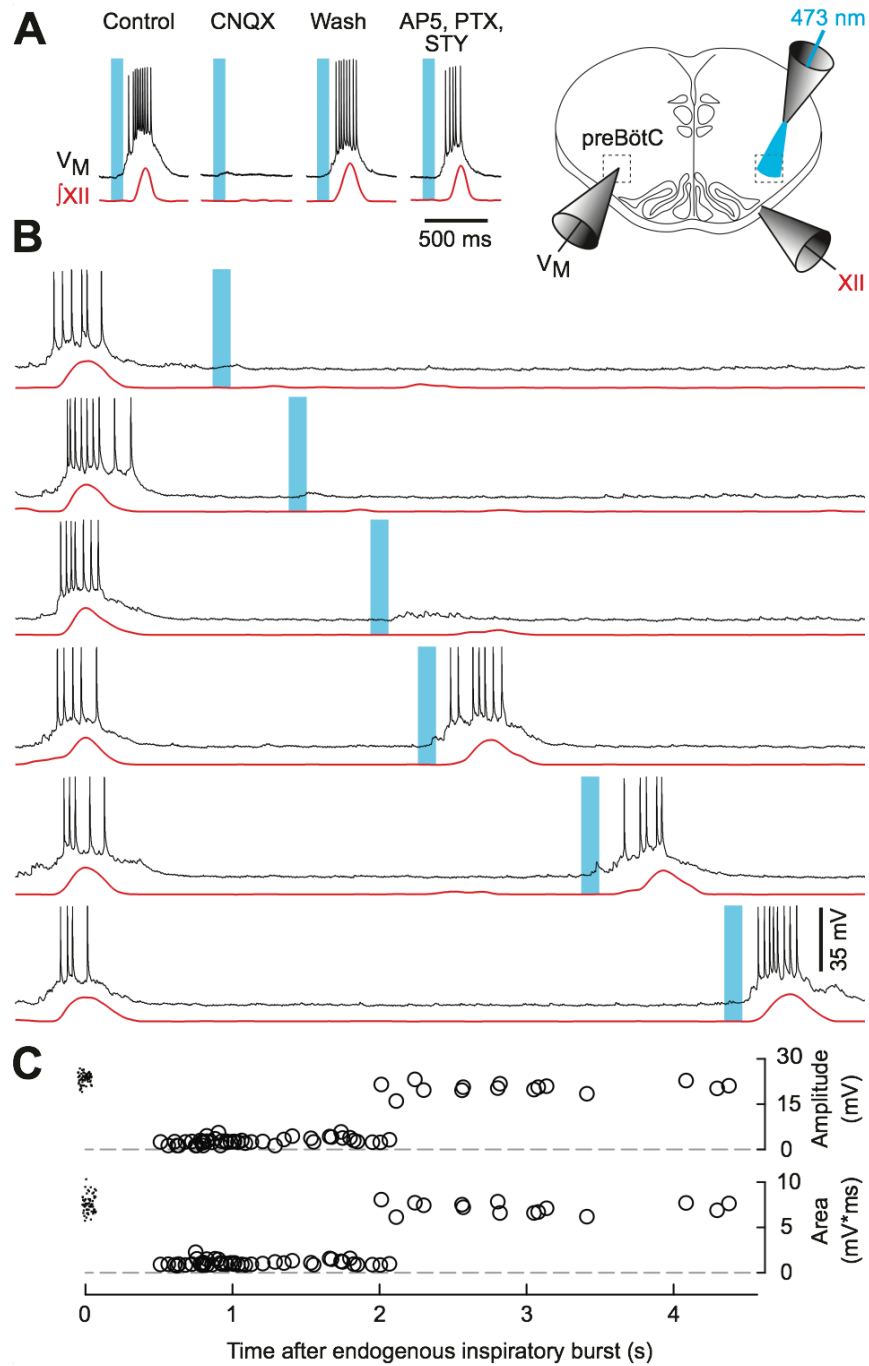
Figure 2.3. Light-evoked inspiratory-like bursts in *Dbx1^CreERT2; Rosa26^hChR2-tdTomato* mouse slices. A, Pharmacology of evoked bursts, time calibration applies to A. B, Laser pulses delivered at increasing intervals following endogenous inspiratory bursts. Voltage calibration applies to A and B. C, Burst amplitude and area plotted versus the time interval between the endogenous inspiratory burst and stimulus onset. Endogenous control bursts are plotted at the 0 s tick. Time calibration for B and C is the abscissa.

originate from tonic (non-inspiratory) neurons upstream of the preBötC, whose excitatory synaptic properties may differ from excitatory synapses among Dbx1 neurons in the preBötC. Therefore, to further assess the contribution of AMPA receptor desensitization to the refractory period, we pressure-ejected AMPA onto Dbx1 neuron dendrites in five-pulse trains, and then measured transient postsynaptic depolarizations (Fig. 2.4B, left). Whether we compared the first to the second pulse (Fig. 2.4B, black symbols), or the first to the fifth pulse (presumably steady state, Fig. 2.4B, grey symbols), there was no systematic change in the amplitude of the postsynaptic response to AMPA at any pulse interval (n=5 Dbx1 neurons, Friedman test, all p>0.05). These data suggest that AMPA receptor desensitization probably does not account for the refractory period.

We examined presynaptic factors that could contribute to the refractory period. The most common form of short-term synaptic depression involves progressive depletion of the readily releasable pool of synaptic vesicles during bouts of intense neural activity. Because vesicle recycling machinery is Ca^{2+}-sensitive, elevations in presynaptic Ca^{2+} accelerate the refilling of depleted terminals (Dittman and Regehr, 1998; Stevens and Wesseling, 1998; Yang and Xu-Friedman, 2008; Lipstein et al., 2013). Thus, by manipulating extracellular Ca^{2+} we aimed to influence the amount of presynaptic Ca^{2+} that accumulates during an inspiratory burst, and thus the rate of replenishment of expended synaptic
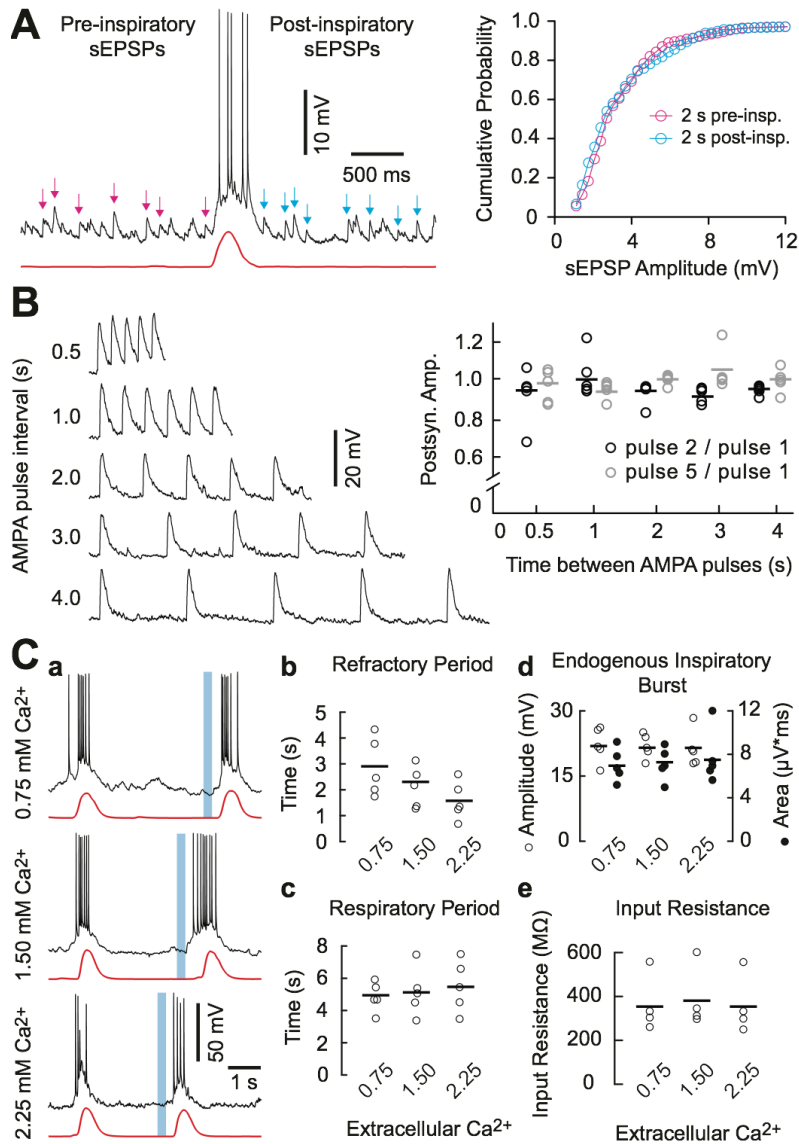
Figure 2.4. Spontaneous EPSPs (sEPSPs), dendritic AMPA pulses, and extracellular Ca^{2+} modulation of the refractory period. A, sEPSPs prior to (magenta) and after (cyan) an endogenous inspiratory burst, and the cumulative probability histogram for sEPSP amplitude. Calibrations apply to A. B, Postsynaptic responses to repetitive dendritic AMPA pulses separated by 4, 3, 2, 1 or 0.5 s (left). The amplitude of the second (black) or fifth (gray) postsynaptic response, normalized to the first response, is plotted for each time interval (right). Bars show means. Voltage calibration to B; time calibration can be inferred by AMPA pulse interval timing. C, Minimum refractory period following an endogenous inspiratory burst (like Figure 3B) plotted for different $[Ca^{2+}]_o$ (a). Voltage and time calibrations apply to C(a). Refractory period (b), respiratory cycle period (c), endogenous inspiratory burst amplitude and area (d), and input resistance (e) are plotted for each $[Ca^{2+}]_o$. Symbols show individual experiments; solid lines represent population means.

47

vesicles. In 0.75 mM Ca^{2+} the refractory period measured 2.88 ± 1.18 s; in 1.50 mM Ca^{2+} it measured 2.22 ± 0.94 s; and in 2.25 mM Ca^{2+} it measured 1.66 ± 0.81 s (Fig. 2.4Ca). The duration of the refractory period is inversely proportional to the level of extracellular Ca^{2+} (Fig. 2.4Cb, n=5, Friedman χ^2=6.4, p=0.04). In contrast, these same changes in extracellular Ca^{2+} caused no significant change in the respiratory cycle period (Fig. 2.4Cc, n=5, Friedman χ^2=0.7, p=0.7), and did not affect the amplitude (n=5 Dbx1 neurons, Friedman χ^2=2.8, p=0.25) or area (n=5 Dbx1 neurons, Friedman χ^2=1.6, p=0.45) of endogenous inspiratory bursts (Fig. 2.4Cd). Ca^{2+} manipulations did not affect the input resistance of Dbx1 preBötC neurons (Fig. 2.4Ce, n=4, Friedman χ^2=0.5, p=0.78). These data indicate that extracellular Ca^{2+} manipulations influence the duration of the refractory period, but do not affect excitability or basic intrinsic properties of Dbx1 preBötC neurons, suggesting that the refractory period and its modulation by extracellular Ca^{2+} cannot be attributed to postsynaptic factors.

2.5 Discussion

Breathing movements emanate from neural activity in a central pattern generator circuit whose core interneurons are known. Dbx1-derived preBötC neurons are bilaterally interconnected glutamatergic interneurons that express membrane properties consistent with rhythmogenic function. *Dbx1* knockout mice form no preBötC and suffer fatal asphyxia at birth (Bouvier et al., 2010;

Gray et al., 2010). Therefore, elucidating the cellular and synaptic basis for rhythmogenesis in Dbx1 preBötC neurons is crucial for understanding the neural origins of the full breathing motor pattern.

We hypothesized that synaptic depression influences the phase transition from inspiratory to post-inspiratory (i.e., early expiratory) activity in Dbx1 preBötC interneurons. To quantify short-term depression, we stimulated midline-crossing axons and observed a progressive diminution of evoked EPSP amplitude and increasing probability of synaptic failure (reaching 50% by the end of the bout). Because the decay time constant of evoked EPSPs was ~100 ms, stimulation rates could not exceed 5 Hz without causing temporal summation and obscuring the analysis. Nonetheless, these data establish that excitatory synapses among Dbx1 preBötC neurons experience short-term depression when activated repetitively. We can infer that in the context of rhythmogenesis, when Dbx1 preBötC neurons discharge 5-20 intra-burst spikes at 15-50 Hz and thus more intensely activate excitatory transmission among the interconnected Dbx1 population, synaptic depression could decrease the magnitude of synaptic potentials by 50-70% and increase the probability of synaptic failure to 10-50%. Therefore, we surmise that synaptic depression could curtail recurrent excitation and thus contribute to inspiratory burst termination, but this remains to be demonstrated.

Activity-dependent synaptic depression could contribute to terminating not only

bursts but also 'burstlets' in the preBötC, which are periodic inspiratory events of lower intensity that do not result in motor output, but have been proposed as a basic substrate of rhythmogenesis (Kam et al., 2013). preBötC neurons generate ~6 spikes per burstlet at average rate of 15 Hz (range 5-28 Hz, see Fig. 6 in Kam et al., 2013) and our results (Fig. 2.2) show that – at a minimum – synaptic potentials could decline by 40% and failure probability could rise to 10% within the constraints of these intra-burstlet spiking parameters.

The mechanisms responsible for inspiratory burst termination and post-inspiratory activity are vigorously debated. The group-pacemaker hypothesis posits that convolved synaptic and intrinsic properties of preBötC neurons mediate inspiratory-expiratory phase transition (Rekling et al., 1996; Rekling and Feldman, 1998). In a mathematical model of the group pacemaker, presynaptic depression can intervene during the inspiratory burst to curb recurrent excitation, which facilitates inspiratory burst termination and promotes the inspiratory-expiratory phase transition (Rubin et al., 2009). Simultaneously, activity-dependent outward currents, namely Na/K ATPase electrogenic pump current (I_{pump}), Na$^+$-dependent K$^+$ current (I_{Na-K}), and ATP-dependent K$^+$ current (I_{K-ATP}), play a complementary role in burst termination and phase transition. These outward currents in preBötC neurons were experimentally identified (Del Negro et al., 2009; Krey et al., 2010), while the potential role for short-term synaptic depression remained an untested prediction of the group-pacemaker

model. I_{pump}, I_{Na-K}, and I_{K-ATP} relax within 15-300 ms following burst termination, which is too short to explain the refractory period in vitro that measured 2 s in response to hChR2activation, but measured ~1 s when a bolus of AMPA was administered unilaterally to the preBötC following inspiratory burst termination (Del Negro *et al.*, 2009). This shorter refractory period is most likely attributable to the stronger stimulus, AMPA application depolarized preBötC neurons by 40 mV and then slowly decayed for 1 min, whereas hChR2 depolarized Dbx1 preBötC neurons <10 mV for exactly 100 ms. In both cases the refractory period outlasts postsynaptic contributions of I_{pump}, I_{Na-K}, and I_{K-ATP}. Therefore, we propose that activity-dependent outward currents and synaptic depression act in concert to influence inspiratory-expiratory phase transition, terminating the inspiratory burst and then causing a transient phase of post-inspiratory quiescence in the network.

Could this mechanism identified in models and in vitro apply in vivo? We observed a ~2 s refractory period following inspiratory bursts, which comprises 25-33% of the respiratory cycle period in vitro. By optogenetically stimulating the preBötC in adult rats in vivo, Alsahafi et al. (2015) recently documented a refractory period of 200-400 ms following inspiration, which comprises ~25-60% of the breathing cycle period. The refractory period measured in vitro constitutes the same proportion of the cycle period as the refractory period measured in vivo, suggesting that the refractory period is a real phenomenon,

and not an artifact of the in vitro preparation. Thus, the biophysical mechanisms we identify in vitro could govern the inspiratory-expiratory phase transition in vivo as well.

The most common form of short-term synaptic depression involves presynaptic vesicle depletion during high-frequency activity. Manipulations of Ca^{2+}, which affect release and recovery processes (Neher and Sakaba, 2008), modulated the refractory period during the post-inspiratory phase but did not affect respiratory cycle period, inspiratory burst magnitude, or the input resistance of Dbx1 preBötC neurons (Fig. 2.4). The readily releasable vesicle pool recovery time varies from hundreds of milliseconds to seconds depending on the experimental model (Stevens and Tsujimoto, 1995; Hosoi et al., 2007; Cohen and Segal, 2011). The refractory period in vitro, and the refractory period Alsahafi et al. (2015) measured in vivo are within this range, suggesting that vesicle depletion is a viable explanation for the lack of synaptic efficacy following inspiratory bursts in vitro or inspiration in vivo.

AMPA receptor desensitization is unlikely to contribute on the time scale associated with the refractory period based on measurements of sEPSPs before and immediately after inspiratory bursts, as well as the lack of modulation of postsynaptic responses to repetitive AMPA pulses. However, it remains possible that we measured sEPSPs from a source extrinsic to the preBötC; for example, from an upstream tonic source of excitation to the

preBötC whose postsynaptic AMPA receptors do not exhibit the same biophysical properties as AMPA receptors involved in recurrent excitation. Further, receptors may desensitize during bursts (and thus assist in burst termination) but then recover faster than could be measured using pressure-ejection techniques where the decay kinetics of post-synaptic response precluded pulse rates in excess of 2 Hz. It is also possible that some portion of AMPA receptors targeted by local AMPA application are not inspiratory modulated, therefore we cannot rule out postsynaptic effects entirely.

Conceptual models of respiratory rhythm often feature obligatory roles for postsynaptic inhibition in inspiratory-expiratory phase transition. The present results indicate that excitatory synaptic dynamics of core rhythmogenic Dbx1 interneurons could influence inspiratory burst termination and the quiescent post-inspiratory phase of the respiratory cycle, which should be added to existing frameworks for analysis and models of breathing's neural bases.

2.6 References

Alsahafi Z, Dickson CT, Pagliardini S (2015) Optogenetic excitation of preBötzinger Complex neurons potently drives inspiratory activity in vivo. J Physiol.

Bianchi AL, Denavit-Saubié M, Champagnat J (1995) Central control of breathing in mammals: neuronal circuitry, membrane properties, and neurotransmitters. Physiol Rev 75:1–45.

Bouvier J, Thoby-Brisson M, Renier N, Dubreuil V, Ericson J, Champagnat J, Pierani A, Chédotal A, Fortin G (2010) Hindbrain interneurons and axon guidance signaling critical for breathing. Nat Neurosci 13:1066–1074.

Brockhaus J, Ballanyi K (1998) Synaptic inhibition in the isolated respiratory network of neonatal rats. Eur J Neurosci 10:3823–3839.

Carroll MS, Ramirez J-M (2013) Cycle-by-cycle assembly of respiratory network activity is dynamic and stochastic. J Neurophysiol 109:296–305.

Carroll MS, Viemari J-C, Ramirez J-M (2013) Patterns of inspiratory phase-dependent activity in the in vitro respiratory network. J Neurophysiol 109:285–295.

Cohen D, Segal M (2011) Network bursts in hippocampal microcultures are terminated by exhaustion of vesicle pools. J Neurophysiol 106:2314–2321.

Del Negro CA, Kam K, Hayes JA, Feldman JL (2009) Asymmetric control of inspiratory and expiratory phases by excitability in the respiratory network of neonatal mice in vitro. J Physiol 587:1217–1231.

Dittman JS, Regehr WG (1998) Calcium dependence and recovery kinetics of presynaptic depression at the climbing fiber to Purkinje cell synapse. J Neurosci Off J Soc Neurosci 18:6147–6162.

Feldman JL, Del Negro CA, Gray PA (2013) Understanding the rhythm of breathing: so near, yet so far. Annu Rev Physiol 75:423–452.

Funk GD, Smith JC, Feldman JL (1993) Generation and transmission of respiratory oscillations in medullary slices: role of excitatory amino acids. J Neurophysiol 70:1497–1515.

Gray PA, Hayes JA, Ling GY, Llona I, Tupal S, Picardo MCD, Ross SE, Hirata T, Corbin JG, Eugenín J, Del Negro CA (2010) Developmental origin of preBötzinger complex respiratory neurons. J Neurosci Off J Soc Neurosci 30:14883–14895.

Hosoi N, Sakaba T, Neher E (2007) Quantitative analysis of calcium-dependent vesicle recruitment and its functional role at the calyx of Held synapse. J Neurosci Off J Soc Neurosci 27:14286–14298.

Janczewski WA, Tashima A, Hsu P, Cui Y, Feldman JL (2013) Role of inhibition in respiratory pattern generation. J Neurosci Off J Soc Neurosci 33:5454–5465.

Kam K, Worrell JW, Ventalon C, Emiliani V, Feldman JL (2013) Emergence of population bursts from simultaneous activation of small subsets of preBötzinger complex inspiratory neurons. J Neurosci Off J Soc Neurosci 33:3332–3338.

Krey RA, Goodreau AM, Arnold TB, Del Negro CA (2010) Outward Currents Contributing to Inspiratory Burst Termination in preBötzinger Complex Neurons of Neonatal Mice Studied in Vitro. Front Neural Circuits 4:124.

Lipstein N, Sakaba T, Cooper BH, Lin K-H, Strenzke N, Ashery U, Rhee J-S, Taschenberger H, Neher E, Brose N (2013) Dynamic control of synaptic vesicle replenishment and short-term plasticity by Ca(2+)-calmodulin-Munc13-1 signaling. Neuron 79:82–96.

Moore JD, Deschênes M, Furuta T, Huber D, Smear MC, Demers M, Kleinfeld D (2013) Hierarchy of orofacial rhythms revealed through whisking and breathing. Nature 497:205–210.

Neher E, Sakaba T (2008) Multiple roles of calcium ions in the regulation of

neurotransmitter release. Neuron 59:861–872.

Pace RW, Mackay DD, Feldman JL, Del Negro CA (2007) Inspiratory bursts in the preBötzinger complex depend on a calcium-activated non-specific cation current linked to glutamate receptors in neonatal mice. J Physiol 582:113–125.

Rekling JC, Champagnat J, Denavit-Saubié M (1996) Electroresponsive properties and membrane potential trajectories of three types of inspiratory neurons in the newborn mouse brain stem in vitro. J Neurophysiol 75:795–810.

Rekling JC, Feldman JL (1998) PreBötzinger complex and pacemaker neurons: hypothesized site and kernel for respiratory rhythm generation. Annu Rev Physiol 60:385–405.

Ren J, Greer JJ (2006) Modulation of respiratory rhythmogenesis by chloride-mediated conductances during the perinatal period. J Neurosci Off J Soc Neurosci 26:3721–3730.

Richter DW (1982) Generation and maintenance of the respiratory rhythm. J Exp Biol 100:93–107.

Ruangkittisakul A, Kottick A, Picardo MCD, Ballanyi K, Del Negro CA (2014) Identification of the pre-Bötzinger complex inspiratory center in calibrated "sandwich" slices from newborn mice with fluorescent Dbx1 interneurons. Physiol Rep 2.

Rubin JE, Hayes JA, Mendenhall JL, Del Negro CA (2009) Calcium-activated nonspecific cation current and synaptic depression promote network-dependent burst oscillations. Proc Natl Acad Sci U S A 106:2939–2944.

Sherman D, Worrell JW, Cui Y, Feldman JL (2015) Optogenetic perturbation of preBötzinger complex inhibitory neurons modulates respiratory pattern. Nat Neurosci 18:408–414.

Smith JC, Ellenberger HH, Ballanyi K, Richter DW, Feldman JL (1991) Pre-Bötzinger complex: a brainstem region that may generate respiratory rhythm in mammals. Science 254:726–729.

Stevens CF, Tsujimoto T (1995) Estimates for the pool size of releasable quanta at a single central synapse and for the time required to refill the pool. Proc Natl Acad Sci U S A 92:846–849.

Stevens CF, Wesseling JF (1998) Activity-dependent modulation of the rate at which synaptic vesicles become available to undergo exocytosis. Neuron 21:415–424.

Wallén-Mackenzie A, Gezelius H, Thoby-Brisson M, Nygård A, Enjin A, Fujiyama F, Fortin G, Kullander K (2006) Vesicular glutamate transporter 2 is required for central respiratory rhythm generation but not for locomotor central pattern generation. J Neurosci Off J Soc Neurosci 26:12294–12307.

Yang H, Xu-Friedman MA (2008) Relative roles of different mechanisms of depression at the mouse endbulb of Held. J Neurophysiol 99:2510–2521.

CHAPTER 3: RNA-Seq gene expression analysis of preBötzinger complex neurons in neonatal mice

3.1 Abstract

RNA-Sequencing (RNA-Seq) has emerged as a powerful tool to describe the presence and quantity of RNA in a biological sample. Here we use RNA-Seq to generate a gene expression profile for brainstem interneurons in the specialized respiratory rhythmogenic site preBötzinger Complex (preBötC). We compared preBötC neurons derived from progenitors that express the transcription factor Dbx1 (which constitute the rhythmogenic preBötC core) with non-Dbx1 derived neurons (which presumably support other respiratory functions, such as coordinating inspiratory and expiratory phases of the breathing cycle, as well as sensorimotor integration). We describe the total abundance of messenger RNA (mRNA) in these populations, including genes that encode for neuropeptides and peptide receptors, ion channels, integral membrane proteins, and transcription factors. Despite knowing the location and genetic identity of interneurons that comprise the preBötC core, the cellular mechanisms that underlie respiratory rhythmogenesis are incompletely understood. These data identifying specific subunits for ion channels, transporters, and ATPase pumps that govern the excitable properties of neurons can be exploited to manipulate the physiology of Dbx1 preBötC neurons (and non-Dbx1 counterparts) and thus test their role(s) in respiratory neurobiology. Further, the novel genetic markers

we reveal in these neuron types may provide an unanticipated roadmap for generating experimentally testable predictions regarding preBötC structure and function.

3.2 Introduction

Neural rhythms that drive inspiratory breathing movements in mammals emanate from the brainstem preBötzinger complex (preBötC) (Smith et al., 1991; Feldman et al., 2013). Neurons derived from Dbx1-expressing progenitors (hereafter referred to as Dbx1 neurons) comprise its rhythmogenic core (Bouvier et al., 2010; Gray et al., 2010; Picardo et al., 2013; Wang et al., 2014; Cui et al., 2016; Koizumi et al., 2016; Vann et al., 2016). Although we know the site (preBötC) and genetic cell class (Dbx1) at the point of origin of respiratory rhythm, the mechanisms of rhythmogenesis remain incompletely understood.

Intracellular and patch-clamp recording studies have characterized intrinsic membrane properties in preBötC neurons generally, and Dbx1 preBötC neurons in particular. Na^+, K^+, mixed cationic, and Ca^{2+} channels, as well as membrane pumps and transporters contribute to, and influence, the cellular and synaptic neural mechanisms of respiratory rhythm generation (Ramirez and Richter, 1996; Feldman et al., 2013; Richter and Smith, 2014). However, testing the relative roles of channels, transporters, and pumps in rhythm generation has relied on promiscuous pharmacology, and has often led to inconclusive

results. We argue that more definitive experimental approaches would be possible if the specific subunits and genes that underlie rhythmogenic conductances and integral membrane proteins were known. Knowledge of the preBötC transcriptome – the expressed genes and the quantity of their respective messenger RNA – could be exploited to develop targeted experiments that manipulate ion channels (specific subunits and isoforms), pumps, and transporters, with the added benefit of uncovering novel genes that might influence preBötC development, as well as generate or regulate respiratory rhythm.

Here we provide the first RNA-Seq gene expression profile for preBötC neurons. We determine the presence and quantity of transcribed RNA in both Dbx1-derived (Dbx1$^+$) and non-Dbx1-derived (Dbx1$^-$) preBötC neurons. Further, we determine which genes are differentially expressed in Dbx1$^+$ and Dbx1$^-$ populations to identify distinguishing characteristics. With the publication of this dissertation and resulting manuscript, these data will be made publicly available in an open access database, which enables users to exploit these data in custom ways, and analyze gene expression independently. This study shows gene expression in preBötC neurons, and can be used to design hypothesis driven studies addressing the role of transcription factors in development of the preBötC, as well as cellular and molecular mechanisms that animate respiratory rhythm.

3.3 Materials and Methods

Animals: All procedures were approved by the Institutional Animal Care and Use Committee at the College of William & Mary. To identify Dbx1-derived preBötC neurons, female tamoxifen-inducible Dbx1 Cre-driver mice ($Dbx1^{CreERT2}$; Hirata et al., 2009) were mated with male reporter mice whose $Rosa26$ locus was modified by targeted insertion of a $loxP$-flanked STOP cassette followed by a gene for the fluorescent protein $tdTomato$ ($Rosa26^{tdTomato}$, stock no. 007905; The Jackson Laboratory). Tamoxifen (22.5 mg/kg body mass) was administered to pregnant dams at embryonic day 9.5. In $Dbx1^{CreERT2}$; $Rosa26^{tdTomato}$ mice, Cre-mediated recombination resulted in cytosolic tdTomato expression in cells derived from Dbx1-expressing progenitors.

Medullary slices: Neonatal mice (postnatal day 0-1) of both sexes were anesthetized by hypothermia and their neuraxes were dissected in ice-cold artificial cerebrospinal fluid (aCSF) containing the following (in mM): 124 NaCl, 3 KCl, 1.5 $CaCl_2$, 1 $MgSO_4$, 25 $NaHCO_3$, 0.5 NaH_2PO_4, and 30 dextrose equilibrated with 95% O_2/5% CO_2, pH 7.4. Transverse medullary slices (500 μm) that expose the preBötC on the rostral surface were prepared with a vibratome and perfused with ice-cold aCSF at 5 ml/min.

Neuron extraction: Dbx1-derived preBötC neurons were identified using epifluorescence and extracted under bright-field imaging on a fixed-stage microscope. Heat-sterilized micropipettes were fabricated from borosilicate

capillary glass (1.50 mm outer diameter, 0.86 mm inner diameter). The micropipettes were void of solution prior to the extraction. When a seal was formed with the cell membrane, negative pressure was applied to draw a single neuron into the tip of the micropipette. Tips containing the sampled neurons were immediately broken in sterile RNase/DNase-free tubes submersed in liquid nitrogen until a total of 15 neurons were collected. Each sample of 15 neurons (n=6) was collected from a different animal.

cDNA synthesis: The volume in each tube was made to equal 10.5 µl by adding nuclease-free water and lysis buffer with RNase inhibitor included in the SMART-Seq v4 ultra low input RNA kit for Sequencing (634889, Clontech, Mountain View, CA). The contents were incubated with sonication for 5 min to lyse the neurons and release cytoplasmic RNA, and then transferred to a 0.2-ml RNase-free PCR tube. First strand cDNA was synthesized by performing reverse transcription in a thermal cycler (42°C for 90 min, 70°C for 10 min) and was then primed by the 3' SMART-Seq CDS Primer IIA and used the SMART-Seq v4 Oligonucleotide for template switching at the 5' end of the transcript. cDNA was then amplified by LD-PCR from the SMART sequences introduced by 3' SMART-Seq CDS Primer IIA and the SMART-Seq v4 oligonucleotide in a heated thermal cycler (95°C for 1 min; 17 cycles of 98°C for 10 s, 65°C for 30 sec, 68°C for 3 min; 72°C for 10 min). PCR-amplified cDNA was purified by immobilization on Agencourt AMPure XP beads (A63880, Beckman Coulter,

Brea, CA), which were then washed with 80% ethanol and cDNA was eluted with elution buffer. The amplified cDNA was validated using the Agilent 2100 Bioanalyzer and Agilent's High Sensitivity Kit (5067-4626, Agilent Technologies, Santa Clara, CA) and its concentration was determined using Qubit dsDNA High-sensitivity Assay Kit (Molceular Probes). The full-length cDNA output was processed with the Nextera Library Preparation kit (FC-131-1024, Illumina, San Diego, CA) to obtain cDNA libraries for RNA-Seq experiments.

Sequence analysis: Six cDNA libraries (three biological replicates from Dbx1$^+$ samples and three biological replicates from Dbx1$^-$ samples) were submitted to the DNA sequencing center at Brigham Young University (Provo, UT) for sequencing. We received 30 million single-end reads per sample, which were sequenced using an Illumina HiSeq 2500. We received read sequences and quality scores in the form of FASTQ files. We employed the Galaxy Cluster at Johns Hopkins University (https://usegalaxy.org/) to align single-end reads to the mm10 mouse reference genome (University of California, Santa Cruz) using Tophat2. This resulted in binary alignment/map (BAM) files. The BAM files were sorted using SAMtools (a set of utilities for processing short DNA sequence read alignments; http://www.htslib.org/download/) and HTSeq-count was used to map the reads to genes. A customized Python script read the ENSEMBL mouse annotation database (http://useast.ensembl.org/) to extract the total exon length for each gene and normalize the reads to units of reads per

kilobase of transcript per million mapped reads (RPKM). Differential gene expression analysis was performed on the HTSeq-count output files using DESeq2 (Love et al., 2014) using the default settings. Default output values include the mean of the raw reads across the six samples (Mean), Log2FoldChange (L2FC), which is the difference between raw read values in Dbx1$^+$ and Dbx1$^-$ samples (negative L2FC indicates higher expression in Dbx1$^-$ population), and adjusted p values (Adj. p value). Heat maps for visual display of gene expression were created by performing a logarithmic transformation of RPKM values using the formula (Heat map value = $\log_{10}(1+\text{RPKM})$). All data are presented as mean ± standard deviation.

3.4 Results and Discussion

To characterize gene expression in preBötC neurons, we prepared brainstem sections (500 μm-thick) from *Dbx1*$^{\text{CreERT2}}$; *Rosa26*$^{\text{tdTomato}}$ mice (n=6, P0-1) that exposed the preBötC on the rostral surface, which was verified by its position between the semi-compact division of the nucleus ambiguus and the dorsal boundary of the principal loop of the inferior olive (Fig. 3.1A) (Ruangkittisakul et al., 2014). We identified Dbx1 neurons by native tdTomato fluorescence and then harvested them one at a time using glass micropipettes (Fig. 3.1B). We pooled 15 neurons per sample in order to diminish the effects of cell-to-cell heterogeneity, and thereby maximize the number of detected genes in Dbx1$^+$ and Dbx1$^-$ populations. We collected three separate samples from different

animals for Dbx1$^+$ and Dbx1$^-$ neuron populations (six samples in total) to analyze differential gene expression (Fig. 3.1C).

We used the SMART-Seq v4 ultra low input RNA kit for cell lysis, cDNA synthesis and amplification. We used a bioanalyzer to validate that fragment
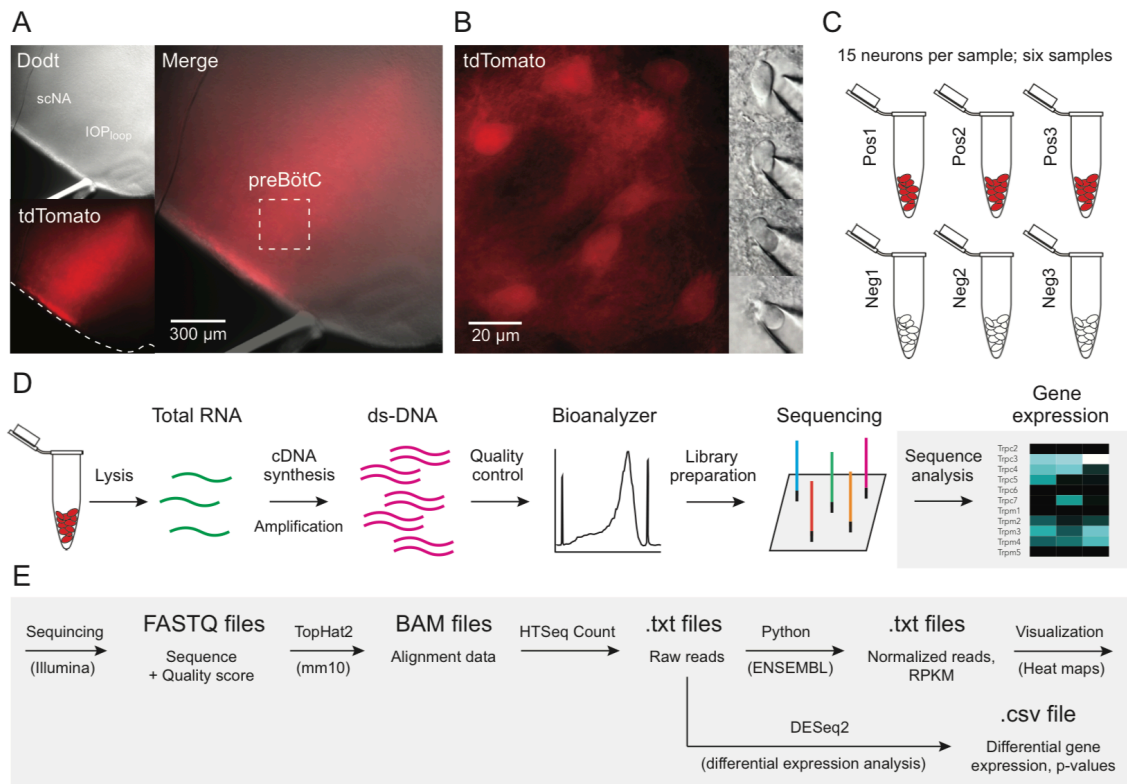
Figure 3.1. RNA-Seq extraction and analysis pipeline. A, Rostral slice surface from a *Dbx1^{CreERT2}; Rosa26^{tdTomato}* mouse pup showing hypoglossal motor nucleus (XII), semi-compact division of the nucleus ambiguus (scNA), and the principal loop of the inferior olive (IO$_{loop}$), sites co-localized with the preBötC. Dotted box marks the preBötC. B, Dbx1-derived preBötC neurons were identified based on native tdTomato fluorescence (left) and extracted with glass micripipettes (right). C, Fifteen Dbx1$^+$ and Dbx1$^-$ preBötC neurons were extracted per sample; samples were collected in triplicates. D-E, cDNA synthesis and analysis pipeline.

length and distribution (average fragment size ~600 bp with sharp peak), and then ligated adapters for sequencing using the Nextera library preparation kit

(Fig. 3.1D). To test for the possibility that background RNA present outside of cells in the milieu bathing the specimen contaminated our samples, we performed mock cellular extractions as a negative control, bringing micropipettes into contact with the surface of the slice without collecting cells. We harvested these pipettes and performed cDNA synthesis and amplification in the same way as our cell samples. Further, we performed cDNA synthesis and amplification using distilled H_2O. The cell-extraction samples contained 1481 ± 352 pg/µl (n=6) of amplified cDNA, while the negative control contained 93.41 pg/µl, and the distilled H_2O control contained 23.18 pg/µl. This suggests that our transcriptome database represents cytoplasmic mRNA in preBötC neurons and was not contaminated by extraneous genetic material.

Sequencing with the Illumina HiSeq 2500 generated an average of 15.3 ± 1.2 million (n=6) single-end reads per sample, with an average read length of 49.5 bp (range: 35-50 bp). Read sequences were aligned to the mm10 mouse genomic database using Tophat2. The average mapping rate was 85 ± 7% (n=6) of total input reads. RPKM (reads per kilobase of transcript per million mapped reads) values were generated for each gene and sample by normalizing for exon length using the ENSEMBL mouse gene annotation database. We generated heat maps for visual display using logarithmic transformation of RPKM values, and analyzed differential gene expression between Dbx1^{+} and Dbx1^{-} neurons using DESeq2 (Fig. 3.1E).

Dbx1-expressing progenitors give rise to preBötC neurons and glia, which can be visually distinguished by their distinct morphologies (see Chapter 1 of this dissertation). In addition to these visual criteria, to confirm that we extracted neurons, we probed the transcriptome data for microglia, oligodendrocyte, astrocyte, and neuron-specific markers (Cahoy et al., 2008; Zhang et al., 2014). The neuron markers exhibited high expression levels, while the markers for the other cell types were undetectable or very low (Fig. 3.2). These data, combined with the negative control data and cDNA fragment distribution (indicating that RNA was not substantially degraded during the extraction process) suggest that we constructed a high-quality preBötC neuron transcriptome database.
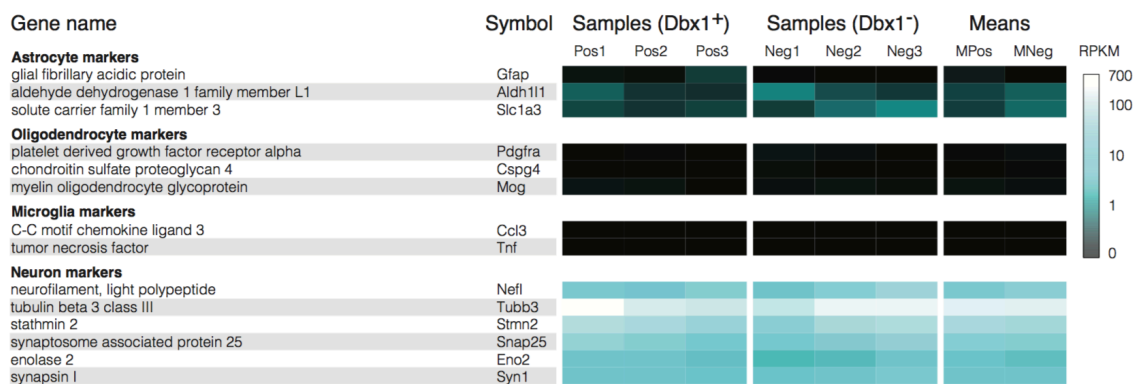
Figure 3.2. Heat map displaying the detection levels for known neuron and glia markers in Dbx1$^+$ and Dbx1$^-$ preBötC neurons.

An exhaustive review of gene expression for Dbx1$^+$ and Dbx1$^-$ preBötC neurons is beyond the scope of this dissertation, and unfeasible given the number of genes identified. Here, we examine gene expression of a pertinent subset of

respiratory markers in Dbx1$^+$ preBötC neurons, and comment on a subset of differentially expressed genes.

Peptides and peptide receptors. We examined our transcriptome database for peptides and peptide receptors that modulate respiratory rhythm. We observed high levels of somatostatin and somatostatin receptor gene expression, consistent with previous studies describing somatostatin labeling of preBötC rhythmogenic core neurons, or their motor pattern-forming elements (Tan et al., 2008; Pantaleo et al., 2011; Cui et al., 2016) (Fig. 3.3).

We also observed tachykinin receptor gene expression (Fig. 3.3), consistent with a strong thread in the literature demonstrating that neurokinin 1 receptor-expressing preBötC neurons are required for normal breathing (Gray et al., 2001; McKay et al., 2005), and that neurokinin 1 receptors are highly expressed in Dbx1-derived neurons of the preBötC (Gray et al., 2010).

Opiate-induced respiratory depression is well documented, and is mediated (in part) by opioid receptor agonists acting on cognate receptors expressed in the preBötC (Gray et al., 1999; Mellen et al., 2003; Montandon et al., 2011). We found that preBötC neurons express delta-, kappa-, and mu-opioid receptor genes, as well as the gene for the endogenous opioid proenkephalin (Fig. 3.3).
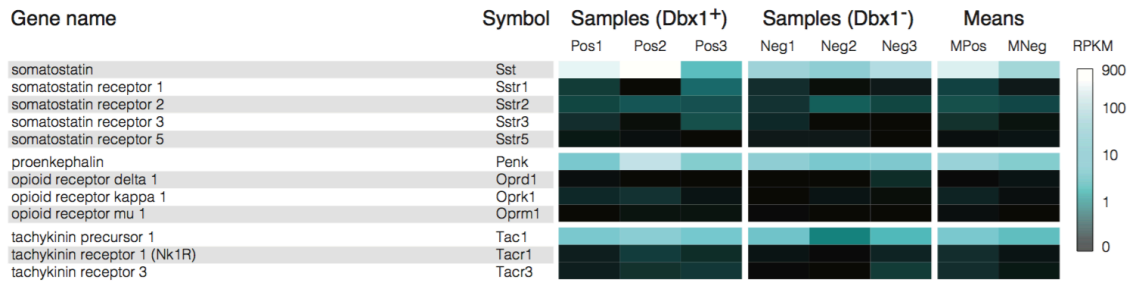
Figure 3.3. Heat map displaying the detection levels of respiratory-related peptides and peptide receptors.

Excitatory and inhibitory markers. The generation and transmission of inspiratory breathing rhythm depends critically on AMPA receptor-mediated excitatory synaptic interactions (Funk et al., 1993; Wallén-Mackenzie et al., 2006), and Dbx1-derived preBötC neurons are almost exclusively glutamatergic (Bouvier et al., 2010; Gray et al., 2010). Although postsynaptic inhibition is not required for rhythmogenesis (Brockhaus and Ballanyi, 1998; Ren and Greer, 2006; Janczewski et al., 2013), inhibitory neurons exist in the preBötC and likely serve to shape the pattern of respiratory motor output and mediate sensorimotor integration (Janczewski et al., 2013; Sherman et al., 2015). We observed high levels of gene expression for excitatory markers like glutamate synthesizing enzymes, transporters, and receptors in Dbx1$^+$ neurons (Fig. 3.4). However, we were surprised to observe gene expression for inhibitory amino acid synthesizing enzymes and transporters in Dbx1$^+$ neurons as well (Fig 3.5). These expression levels were commensurate with Dbx1$^-$ neurons, which was puzzling, because we expected Dbx1$^+$ neurons to be exclusively glutamatergic,

and non-Dbx1 neurons to be exclusively inhibitory. These data could indicate that either: 1) Dbx1$^+$ neurons are truly glutamatergic but express mRNA for inhibitory markers that is not translated (Cao et al., 1996), or 2) that a non-negligible subset of Dbx1 preBötC neurons are inhibitory. That subset of possibly inhibitory Dbx1 neurons is conceivable based on anatomical counts in the first two reports of Dbx1 preBötC neurons. Bouiver et al. (2010) showed that 82% of Dbx1 preBotC neurons expressed VGLUT2 (glutamatergic marker)

Gene name	Symbol	Samples (Dbx1$^+$)			Samples (Dbx1$^-$)			Means		RPKM
		Pos1	Pos2	Pos3	Neg1	Neg2	Neg3	MPos	MNeg	
glutamate-ammonia ligase	Glul									
glutamate dehydrogenase 1	Glud1									
solute carrier family 17 member 6 (vesicular glutamate transporter 2)	Slc17a6									
glutamate ionotropic receptor AMPA type subunit 1	Gria1									
glutamate ionotropic receptor AMPA type subunit 2	Gria2									
glutamate ionotropic receptor AMPA type subunit 3	Gria3									
glutamate ionotropic receptor AMPA type subunit 4	Gria4									
glutamate ionotropic receptor kainate type subunit 1	Grik1									
glutamate ionotropic receptor kainate type subunit 2	Grik2									
glutamate ionotropic receptor kainate type subunit 3	Grik3									
glutamate ionotropic receptor kainate type subunit 4	Grik4									
glutamate ionotropic receptor kainate type subunit 5	Grik5									
glutamate ionotropic receptor NMDA type subunit 1	Grin1									
glutamate ionotropic receptor NMDA type subunit 2B	Grin2b									
glutamate ionotropic receptor NMDA type subunit 2C	Grin2c									
glutamate ionotropic receptor NMDA type subunit 2D	Grin2d									
glutamate ionotropic receptor NMDA type subunit 3A	Grin3a									
glutamate metabotropic receptor 1 (Group I)	Grm1									
glutamate metabotropic receptor 2 (Group II)	Grm2									
glutamate metabotropic receptor 3 (Group II)	Grm3									
glutamate metabotropic receptor 4 (Group III)	Grm4									
glutamate metabotropic receptor 5 (Group I)	Grm5									
glutamate metabotropic receptor 7 (Group III)	Grm7									
glutamate metabotropic receptor 8 (Group III)	Grm8									

Figure 3.4 Heat map displaying the detection levels of excitatory markers.

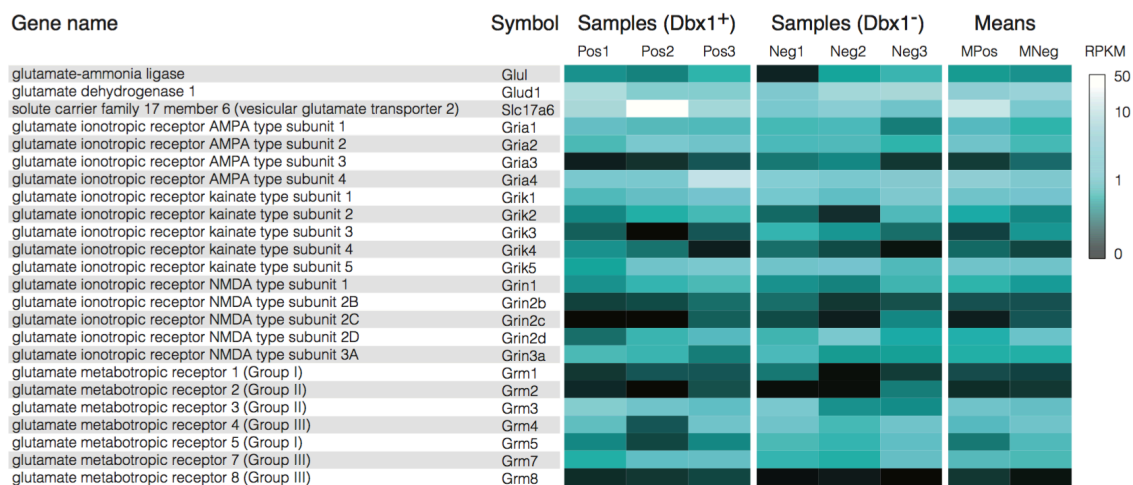and Gray et al. (2010) showed that only 4.7% expressed inhibitory markers. Our RNA-Seq data are broadly consistent with a subset of Dbx1 preBötC neurons that are bona fide inhibitory. Those neurons might be involved in periodic inhibition of the parafacial respiratory group with expiratory function, or to inhibit other orofacial behaviors during ventilation.
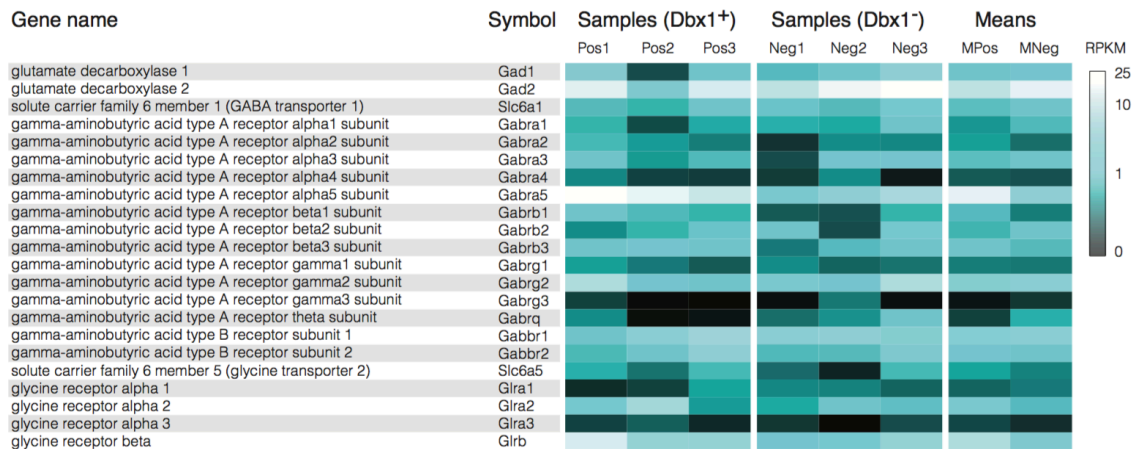
Gene name	Symbol	Samples (Dbx1+)			Samples (Dbx1−)			Means		RPKM
		Pos1	Pos2	Pos3	Neg1	Neg2	Neg3	MPos	MNeg	
glutamate decarboxylase 1	Gad1									25
glutamate decarboxylase 2	Gad2									10
solute carrier family 6 member 1 (GABA transporter 1)	Slc6a1									
gamma-aminobutyric acid type A receptor alpha1 subunit	Gabra1									
gamma-aminobutyric acid type A receptor alpha2 subunit	Gabra2									
gamma-aminobutyric acid type A receptor alpha3 subunit	Gabra3									
gamma-aminobutyric acid type A receptor alpha4 subunit	Gabra4									1
gamma-aminobutyric acid type A receptor alpha5 subunit	Gabra5									
gamma-aminobutyric acid type A receptor beta1 subunit	Gabrb1									
gamma-aminobutyric acid type A receptor beta2 subunit	Gabrb2									
gamma-aminobutyric acid type A receptor beta3 subunit	Gabrb3									
gamma-aminobutyric acid type A receptor gamma1 subunit	Gabrg1									
gamma-aminobutyric acid type A receptor gamma2 subunit	Gabrg2									0
gamma-aminobutyric acid type A receptor gamma3 subunit	Gabrg3									
gamma-aminobutyric acid type A receptor theta subunit	Gabrq									
gamma-aminobutyric acid type B receptor subunit 1	Gabbr1									
gamma-aminobutyric acid type B receptor subunit 2	Gabbr2									
solute carrier family 6 member 5 (glycine transporter 2)	Slc6a5									
glycine receptor alpha 1	Glra1									
glycine receptor alpha 2	Glra2									
glycine receptor alpha 3	Glra3									
glycine receptor beta	Glrb									

Figure 3.5 Heat map displaying the detection levels of inhibitory markers.

Transient receptor potential channels. Inspiratory bursts in the preBötC depend on a calcium-activated nonspecific cationic current (I_{CAN}) (Thoby-Brisson and Ramirez, 2001; Peña et al., 2004; Del Negro et al., 2005; Crowder et al., 2007; Pace et al., 2007; Mironov, 2008; Pace and Del Negro, 2008), which is thought to be mediated by transient receptor potential (TRP) channels. We found that TRP channel genes are expressed in Dbx1+ preBötC neurons, with particularly high expression for TRPC3 (Fig. 3.6). The role of I_{CAN} has not been evaluated in living animals. Further, we do not know which channels give rise to I_{CAN}, or how important they are for respiration. TRPC3 is therefore a novel candidate to exploit in transgenic *in vivo* studies aiming to address the source and importance of I_{CAN} in breathing behavior.
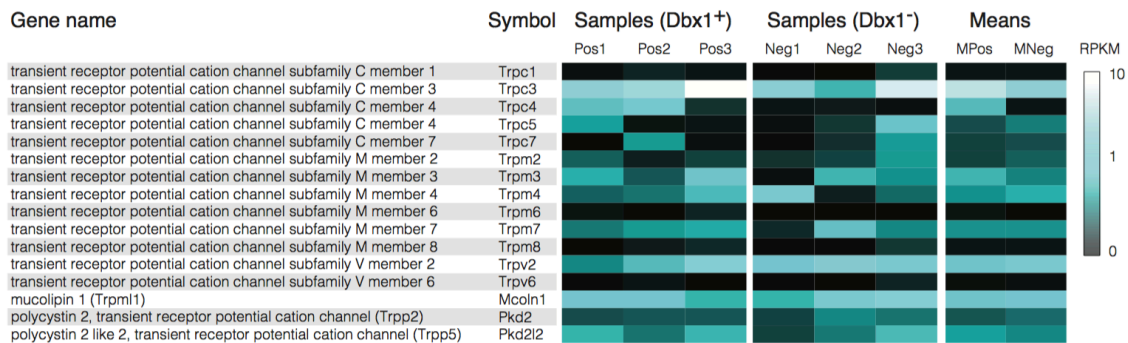
Figure 3.6 Heat map displaying the detection levels of transient receptor potential channels.

Differential gene expression. We performed differential gene expression analysis to determine which genes were more highly expressed in Dbx1^{+} versus Dbx1^{-} populations. We found that 36 genes were differentially expressed (i.e., statistically significant at an adjusted p-value of <0.05), and categorized them into five groups, which included DNA binding proteins (Table 3.1; n=7), structure-related proteins (Table 3.2; n=4), non-protein-coding RNAs (Table 3.3; n=4), enzymes or proteins involved in biochemical cascades (Table 3.4; n=12), and receptors, ion channels, or integral membrane proteins (Table 3.5; n=9). A particularly interesting feature of the list is the number of DNA-binding proteins that were included in the Dbx1^{+} neurons: Mbnl1, Zfp105, Zfp287, Zfp653, and particularly Hif1a. The latter (Hif1a – "hypoxia-inducible factor 1-alpha") is considered the master transcriptional regulator (Wang et al., 1995; Semenza, 1998) managing downstream cascades in cases of hypoxia, and has never before been associated with central rhythm-generating respiratory neurons to our knowledge.

Here we created the first gene expression profile for preBötC neurons. These data demonstrate the presence of known respiratory-related markers, provide insight into which ion channels and subunits might underlie respiratory rhythmogenic currents, and identify novel markers that might influence preBötC development, rhythmogenesis, or response to deviations in normal blood gas concentrations.

Table 3.1. Differential gene expression: DNA binding proteins

Category	Gene	Mean	L2FC	Adj. p value
DNA binding proteins	Gata2	178.02	-3.25	1.68E-07
	Mbnl1	442.27	1.66	5.11E-05
	Zkscan17	318.56	-2.52	1.37E-04
	Zfp105	65.08	2.53	1.66E-03
	Zfp287	76.10	2.30	7.22E-03
	Hif1a	1805.59	1.48	1.53E-02
	Zfp653	127.79	1.88	2.14E-02

Table 3.2. Differential gene expression: Structural proteins

Category	Gene	Mean	L2FC	Adj. p value
Structural proteins	Col12a1	81.15	2.54	1.49E-03
	Gab3	54.78	-2.52	1.66E-03
	Vcl	270.77	-2.11	1.03E-02
	Tmtc4	336.41	1.63	1.53E-02

Table 3.3. Differential gene expression: Non-coding RNAs

Category	Gene	Mean	L2FC	Adj. p value
Non-coding	D930028M14Rik	348.93	-3.76	3.68E-09
	2810468N07Rik	204.11	-3.68	1.27E-08
	Gt(ROSA)26Sor	828.33	-1.14	2.19E-02
	3110052M02Rik	163.93	2.05	2.77E-02

Table 3.4. Differential gene expression: Enzymes / intracellular signaling

Category	Gene	Mean	L2FC	Adj. p value
Enzymes / Intracellular signaling	Cmbl	84.87	-3.42	2.21E-07
	Ctso	137.62	3.06	1.59E-05
	Adssl1	115.70	-2.93	4.97E-05
	Cdr1	674.22	1.42	2.97E-04
	Ebp	386.11	1.53	1.66E-03
	Gnpat	556.52	-1.50	1.74E-03
	Mettl15	64.97	2.50	1.74E-03
	Eya2	76.06	-2.43	2.76E-03
	Pld5	379.95	1.50	2.10E-02
	Ptprm	351.07	1.86	2.35E-02
	Cfp	40.14	2.07	2.77E-02
	Map2k3	158.18	1.69	4.98E-02

Table 3.5. Differential gene expression: Receptors / ion channels

Category	Gene	Mean	L2FC	Adj. p value
Receptors / ion channels	Chrm2	192.54	2.43	3.03E-04
	Gabra5	1625.75	1.16	1.74E-03
	Trpc4	272.83	2.33	3.68E-03
	Adrbk2	569.63	-1.58	9.56E-03
	Sntg2	67.02	2.21	1.35E-02
	Ucp2	468.07	-1.92	1.53E-02
	Htr1a	231.63	-2.05	2.00E-02
	Reep3	133.25	-2.11	2.19E-02
	Vopp1	816.23	-1.02	2.77E-02

3.5 References

Bouvier J, Thoby-Brisson M, Renier N, Dubreuil V, Ericson J, Champagnat J, Pierani A, Chédotal A, Fortin G (2010) Hindbrain interneurons and axon guidance signaling critical for breathing. Nat Neurosci 13:1066–1074.

Brockhaus J, Ballanyi K (1998) Synaptic inhibition in the isolated respiratory network of neonatal rats. Eur J Neurosci 10:3823–3839.

Cahoy JD, Emery B, Kaushal A, Foo LC, Zamanian JL, Christopherson KS, Xing Y, Lubischer JL, Krieg PA, Krupenko SA, Thompson WJ, Barres BA (2008) A transcriptome database for astrocytes, neurons, and oligodendrocytes: a new resource for understanding brain development and function. J Neurosci Off J Soc Neurosci 28:264–278.

Cao Y, Wilcox KS, Martin CE, Rachinsky TL, Eberwine J, Dichter MA (1996) Presence of mRNA for glutamic acid decarboxylase in both excitatory and inhibitory neurons. Proc Natl Acad Sci U S A 93:9844–9849.

Cui Y, Kam K, Sherman D, Janczewski WA, Zheng Y, Feldman JL (2016) Defining preBötzinger Complex Rhythm- and Pattern-Generating Neural Microcircuits In Vivo. Neuron 91:602–614.

Feldman JL, Del Negro CA, Gray PA (2013) Understanding the rhythm of breathing: so near, yet so far. Annu Rev Physiol 75:423–452.

Funk GD, Smith JC, Feldman JL (1993) Generation and transmission of respiratory oscillations in medullary slices: role of excitatory amino acids. J Neurophysiol 70:1497–1515.

Gray PA, Hayes JA, Ling GY, Llona I, Tupal S, Picardo MCD, Ross SE, Hirata T, Corbin JG, Eugenín J, Del Negro CA (2010) Developmental origin of

preBötzinger complex respiratory neurons. J Neurosci Off J Soc Neurosci 30:14883–14895.

Gray PA, Janczewski WA, Mellen N, McCrimmon DR, Feldman JL (2001) Normal breathing requires preBötzinger complex neurokinin-1 receptor-expressing neurons. Nat Neurosci 4:927–930.

Gray PA, Rekling JC, Bocchiaro CM, Feldman JL (1999) Modulation of Respiratory Frequency by Peptidergic Input to Rhythmogenic Neurons in the PreBötzinger Complex. Science 286:1566–1568.

Hirata T, Li P, Lanuza GM, Cocas LA, Huntsman MM, Corbin JG (2009) Identification of distinct telencephalic progenitor pools for neuronal diversity in the amygdala. Nat Neurosci 12:141–149.

Janczewski WA, Tashima A, Hsu P, Cui Y, Feldman JL (2013) Role of inhibition in respiratory pattern generation. J Neurosci Off J Soc Neurosci 33:5454–5465.

Koizumi H, Mosher B, Tariq MF, Zhang R, Koshiya N, Smith JC (2016) Voltage-Dependent Rhythmogenic Property of Respiratory Pre-Bötzinger Complex Glutamatergic, Dbx1-Derived, and Somatostatin-Expressing Neuron Populations Revealed by Graded Optogenetic Inhibition. eNeuro 3.

Li P, Janczewski WA, Yackle K, Kam K, Pagliardini S, Krasnow MA, Feldman JL (2016) The peptidergic control circuit for sighing. Nature 530:293–297.

Love MI, Huber W, Anders S (2014) Moderated estimation of fold change and dispersion for RNA-seq data with DESeq2. Genome Biol 15:550.

McKay LC, Janczewski WA, Feldman JL (2005) Sleep-disordered breathing

after targeted ablation of preBötzinger complex neurons. Nat Neurosci 8:1142.

Mellen NM, Janczewski WA, Bocchiaro CM, Feldman JL (2003) Opioid-induced quantal slowing reveals dual networks for respiratory rhythm generation. Neuron 37:821–826.

Montandon G, Qin W, Liu H, Ren J, Greer JJ, Horner RL (2011) PreBotzinger complex neurokinin-1 receptor-expressing neurons mediate opioid-induced respiratory depression. J Neurosci Off J Soc Neurosci 31:1292–1301.

Pace RW, Mackay DD, Feldman JL, Del Negro CA (2007) Inspiratory bursts in the preBötzinger complex depend on a calcium-activated non-specific cation current linked to glutamate receptors in neonatal mice. J Physiol 582:113–125.

Pantaleo T, Mutolo D, Cinelli E, Bongianni F (2011) Respiratory responses to somatostatin microinjections into the Bötzinger complex and the pre-Bötzinger complex of the rabbit. Neurosci Lett 498:26–30.

Picardo MCD, Weragalaarachchi KTH, Akins VT, Del Negro CA (2013) Physiological and morphological properties of Dbx1-derived respiratory neurons in the pre-Botzinger complex of neonatal mice. J Physiol 591:2687–2703.

Ramirez JM, Richter DW (1996) The neuronal mechanisms of respiratory rhythm generation. Curr Opin Neurobiol 6:817–825.

Ren J, Greer JJ (2006) Modulation of respiratory rhythmogenesis by chloride-mediated conductances during the perinatal period. J Neurosci Off J Soc Neurosci 26:3721–3730.

Richter DW, Smith JC (2014) Respiratory rhythm generation in vivo. Physiol Bethesda Md 29:58–71.

Ruangkittisakul A, Kottick A, Picardo MCD, Ballanyi K, Del Negro CA (2014) Identification of the pre-Bötzinger complex inspiratory center in calibrated "sandwich" slices from newborn mice with fluorescent Dbx1 interneurons. Physiol Rep 2.

Rubin JE, Hayes JA, Mendenhall JL, Del Negro CA (2009) Calcium-activated nonspecific cation current and synaptic depression promote network-dependent burst oscillations. Proc Natl Acad Sci U S A 106:2939–2944.

Semenza GL (1998) Hypoxia-inducible factor 1: master regulator of O2 homeostasis. Curr Opin Genet Dev 8:588–594.

Sherman D, Worrell JW, Cui Y, Feldman JL (2015) Optogenetic perturbation of preBötzinger complex inhibitory neurons modulates respiratory pattern. Nat Neurosci 18:408–414.

Smith JC, Ellenberger HH, Ballanyi K, Richter DW, Feldman JL (1991) Pre-Bötzinger complex: a brainstem region that may generate respiratory rhythm in mammals. Science 254:726–729.

Tan W, Janczewski WA, Yang P, Shao XM, Callaway EM, Feldman JL (2008) Silencing preBötzinger complex somatostatin-expressing neurons induces persistent apnea in awake rat. Nat Neurosci 11:538–540.

Vann NC, Pham FD, Hayes JA, Kottick A, Del Negro CA (2016) Transient Suppression of Dbx1 PreBötzinger Interneurons Disrupts Breathing in Adult Mice. PloS One 11:e0162418.

Wallén-Mackenzie A, Gezelius H, Thoby-Brisson M, Nygård A, Enjin A,

Fujiyama F, Fortin G, Kullander K (2006) Vesicular glutamate transporter 2 is required for central respiratory rhythm generation but not for locomotor central pattern generation. J Neurosci Off J Soc Neurosci 26:12294–12307.

Wang GL, Jiang BH, Rue EA, Semenza GL (1995) Hypoxia-inducible factor 1 is a basic-helix-loop-helix-PAS heterodimer regulated by cellular O2 tension. Proc Natl Acad Sci U S A 92:5510–5514.

Wang X, Hayes JA, Revill AL, Song H, Kottick A, Vann NC, LaMar MD, Picardo MCD, Akins VT, Funk GD, Del Negro CA (2014) Laser ablation of Dbx1 neurons in the pre-Bötzinger complex stops inspiratory rhythm and impairs output in neonatal mice. eLife 3:e03427.

Zhang Y, Chen K, Sloan SA, Bennett ML, Scholze AR, O'Keeffe S, Phatnani HP, Guarnieri P, Caneda C, Ruderisch N, Deng S, Liddelow SA, Zhang C, Daneman R, Maniatis T, Barres BA, Wu JQ (2014) An RNA-sequencing transcriptome and splicing database of glia, neurons, and vascular cells of the cerebral cortex. J Neurosci Off J Soc Neurosci 34:11929–11947.

Conclusion

Dbx1 is currently the best marker for rhythmogenic preBötC neurons. As such, in the first chapter I optimized the delivery of tamoxifen in Dbx1^{CreERT2} mice to maximize neuronal reporter labeling in the preBötC core. I then utilized this Dbx1^{CreERT2} mouse model in the second chapter to investigate the role of excitatory synaptic mechanisms in the production of breathing rhythm. In the third chapter, I created the first gene expression profile for preBötC neurons, which include ion channels and subunits that are pertinent to respiratory physiologists, and I identified novel genetic factors that distinguish Dbx1-derived preBötC neurons from intermingled populations.

The research presented in this dissertation advances our understanding of the neural control of breathing behavior by describing the cellular and molecular composition of the preBötC core as defined by Dbx1-derived neurons, as well as synaptic mechanisms underlying rhythmogenesis.